State-of-Art, Development, and Challenges of Model-Free Predictive Control on Motor Drives

Fengxiang Wang, *Senior Member, IEEE*, Yao Wei, *Member, IEEE*, Jose Rodriguez, *Life Fellow, IEEE*, and Cristian Garcia, *Senior Member, IEEE*

***Abstract*—Model-free predictive control (MFPC) is an essentially robust strategy in motor driving systems, garnering significant attention and research. However, the existing literature lacks a comprehensive analysis of data-driven model design, a critical aspect that directly impacts prediction accuracy and control performance of MFPC. This article innovatively categorizes MFPCs used in motor drives based on data-driven models, systematically investigating various model structures and updating algorithms, and organizes and compares the characteristics of each model. In particular, the challenges faced by MFPC and potential future developments are delved deeply, presenting insights and perspectives that hopefully facilitate future research work in this area.**

***Index Terms*—Adaptability, data-driven model, estimation algorithm, model-free predictive control (MFPC), motor drives.**

I. Introduction

With the rapid development of modern industry and the transportation electrification, motor drives have taken on a pivotal role, and the demand for high-performance control strategies has become even more critical . However, the complex dynamic characteristics and nonlinear behaviors of motors, combined with the effects of external disturbances and internal parameter changes, pose significant challenges to the control strategy for motor drives [1]. To address these challenges, researchers are constantly exploring new control strategies. Model predictive control (MPC), as an advanced control method, has attracted widespread attention in the field of motor drives [2]. MPC employs plant's model to predict future outputs by the rolling optimization (also named receding horizon) concept, and selects the optimal control vector to achieve the desired control objectives. This method can not only effectively handle the multiobjective optimization and uncertainty of the system, but also achieve high-performance control effects in complex environments [3].

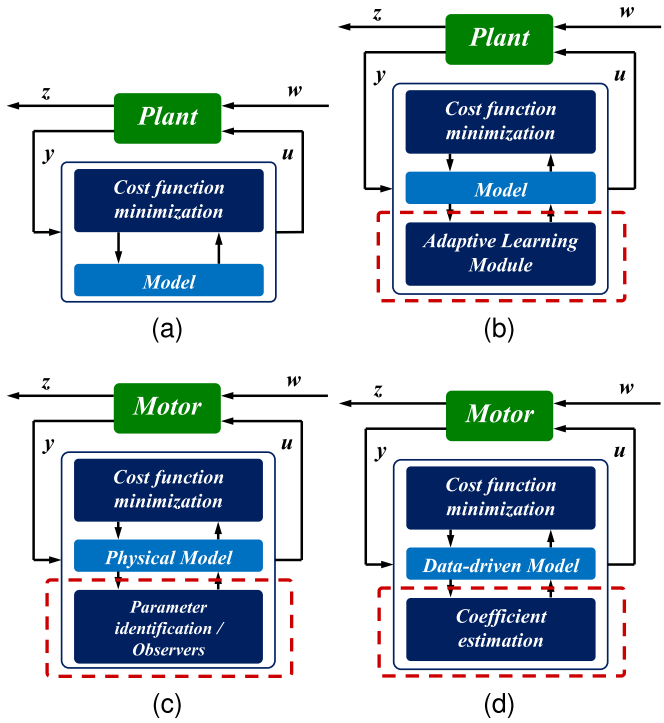

Fig. 1. Development of the predictive control [6]. (a) MBPC framework. (b) Adaptive learning MPC framework. (c) Robustness-enhanced MPC framework in motor drives. (d) Model-free predictive control framework in motor drives.

A. Historical Development for Robustness Enhanced MPC From Prediction Model Perspective

As mentioned previously and as shown in Fig. 1(a), MPC is established and developed based on the fundamental assumption that the mathematical model of the plant is accurately known. Therefore, it can also be referred to as model-based predictive control (MBPC). However, mathematical models often deviate from real systems, particularly in motor drive systems, which are influenced by various operating conditions and environmental

Received 10 October 2024; revised 22 January 2025 and 11 March 2025; accepted 7 April 2025. Date of publication 10 April 2025; date of current version 26 May 2025. This work was supported in part by the National Natural Science Foundation of China under Grant 52277070 and in part by the Fujian Provincial Natural Science Foundation of China under Grant 2024J08125. The work of J. Rodriguez was supported by Agencia Nacional de Investigacion y Desarrollo (ANID) under Grant AFB240002 and Grant 1221293. The work of C. Garcia was supported by ANID/Fondo Nacional de Desarrollo Científico y Tecnológico (FONDECYT) under Grant 1241099, Grant 1231265, and Grant 1230250, and in part by Basal Project AFB240002 (AC3E). Recommended for publication by Associate Editor A. M. Bazzi. *(Corresponding author: Yao Wei.)*

Fengxiang Wang and Yao Wei are with the Quanzhou Institute of Equipment Manufacturing, Haixi Institutes, Chinese Academy of Sciences, Quanzhou 362200, China (e-mail: fengxiang.wang@fjirsm.ac.cn; yao.wei@fjirsm.ac.cn).

Jose Rodriguez is with the Faculty of Engineering, Universidad San Sebastian, Santiago 8370146, Chile (e-mail: jose.rodriguezp@uss.cl).

Cristian Garcia is with the Department of Electrical Engineering, Faculty of Engineering, Universidad de Talca, Curico 3340000, Chile (e-mail: cristian.garcia@utalca.cl).

Color versions of one or more figures in this article are available at https://doi.org/10.1109/TPEL.2025.3559514.

Digital Object Identifier 10.1109/TPEL.2025.3559514

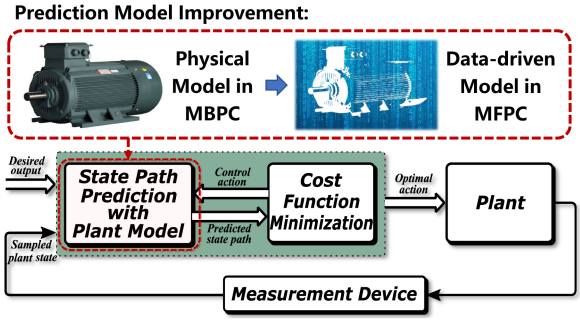

Fig. 2. Implemental principle from MBPC to MFPC.

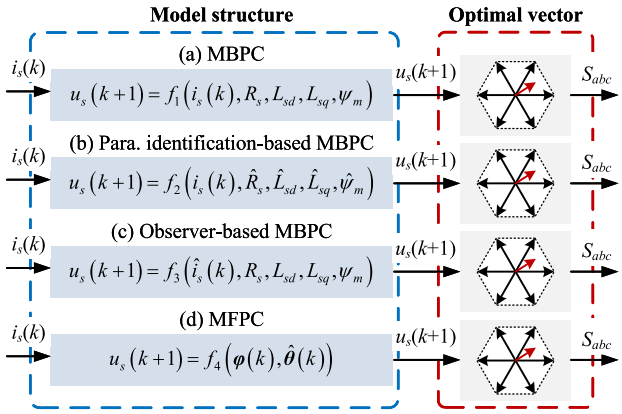

Fig. 3. Simple summary of predictive control with different models.

factors, such as environmental temperature fluctuations, magnetic field coupling, and core saturation. This results in persistent nonlinear dynamic changes in the real system, potentially leading to weak robustness in the control system, and in extreme cases, instability or safety accidents [4]. This poses a serious issue that necessitates resolution in high-end applications [5].

To address this issue, the adaptive learning module within the learning MPC framework, as shown in Fig. 1(b), incorporates mechanisms for parameter identification and state observation, as shown in Fig. 1(c) [6]. These improvements aim to enhance the robustness of MBPC. Parameter identification-based predictive control dynamically estimates physical parameters online, substituting outdated values in the model [7]. Examples include the online identification using the long-term memory recursive least-squares (RLS) algorithm and flux linkage maps in [8]. Concurrently, observer-based predictive control, such as extended state observer (ESO) in [9], disturbance observer (DOB) in [10], and sliding mode observer (SMO) in [11], all consider the negative impact resulting from parameter mismatch as a disturbance. By conducting online observations, accurate estimations of state variables can be achieved, and the system model can be adjusted to mitigate the adverse effects caused by fair robustness [12]. Although these strategies enhance system robustness by mitigating the effects of parameter mismatches, they remain within the MBPC framework and do not completely eliminate the negative impacts.

B. Principle and Current State of Model-Free Predictive Control (MFPC)

MFPC represents a fusion of model-free control techniques and predictive control methodologies. The foundational implemental principle of MFPC is illustrated in Fig. 2, in which the prediction model is crucial as it describes the motion characteristics of the plant and predicts future operating path and states. The primary improvement in MFPC is the prediction model. This approach abandons the reliance on the physical model, instead favoring a data-driven model as depicted in Fig. 1(d), aiming to mitigate the presence of physical parameters and their potential negative impacts [13], [14]. The cornerstone of achieving improved adaptability lies in the careful selection of the model and the estimation of its coefficients. Among the various data-driven models available for motor drives, including but not limited to ultralocal, time-series, and dynamic linearization models, each choice brings unique features and challenges to the realized MFPCs [15]. For a simple comparison between MBPC and MFPC, Fig. 3 provides a straightforward visualization of their fundamental principles. The following is a brief introduction of some typical models in motor drives.

The ultralocal model enjoys widespread adoption in motor drives due to its straightforward implementation and concise structure within the first-order framework [16]. Instead of handling individual unknown terms of the system separately, this model lamps them into a single variable, which online estimates by algebraic algorithms or discrete-time observers, to maintain adaptability [17]. To accommodate varying motor drive demands, the model is refined into a high-order form in [18], advanced form in [19], and affine form in [20]. For enhanced objective quality and prediction precision, multivector selections are adopted within each sampling period, respectively, based on the repetitive predicted ultralocal model [21]. This model's versatility extends to its simultaneous application in both inner and outer control loops, resulting in improved motor drive dynamics and reduced ripples when paired with a quasi-resonant term [22].

The time-series model characterizes the motor driving system as a collection of discrete-time transfer functions, considering the time property of mechanical and inertial components. This class of models encompasses many types, chief among them autoregressive with exogenous input (ARX) and autoregressive moving average (ARMA) [23]. The coefficients of these models are grouped and typically estimated using RLS and its derived algorithms. Based on the ARMA model, a secondary controller is automatically designed, and the control strategy is improved as a two-degree-of-freedom to flexibly adjust the performances in motor drives. However, implementing this model necessitates cautious processor allocation to prevent overrun errors [24].

Utilizing the current gradients associated with candidate vectors, a lookup table (LUT) is listed in MFPC to reflect the operational tendencies and skip the physical terms and nonlinearities of the motor drives. Assuming a similarity between past and future signal gradients, the prediction process can extend into future sampling periods. The design of these tables is flexible, as exemplified in [25], where 2-D tables are constructed to enhance data capacity and improve adaptability. Since this modeling approach relies on signal gradients solely, the stagnant effect

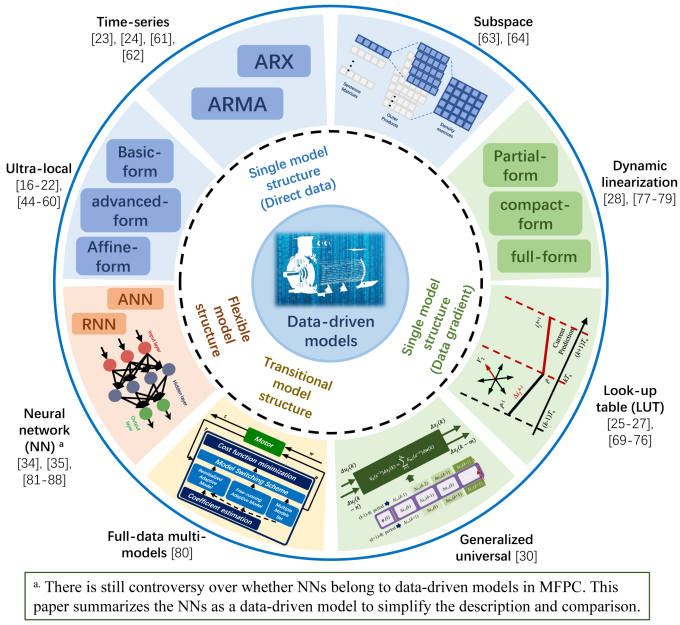

Fig. 4. Classification diagram of some typical data-driven models.

hinders model adaptability and objective quality, particularly when the system employs a low updating frequency or crude sensors. This stagnation poses a significant challenge to enhancing control performance, and recent research has tackled this issue from diverse perspectives [26], [27].

Excepting the aforementioned data-driven models, there exist numerous other data-driven models suitable for MFPC in motor drives, such as the dynamic-linearization model [28], nonparametric current model [29], generalized universal model (GUM) [30], and the models derived from white-box [31]. As motor operating states become more complex, the requirements for a flexible modeling process become paramount. One viable method is the utilization of multiple models, where a set of models is developed for various operating states, and the optimal model is chosen based on a switching strategy that minimizes errors [32]. Nonetheless, motor drives with limited processor resources cannot accommodate numerous data models, limiting their adaptability to complex operating states. To address this, adaptive data-driven models, such as the adaptive ultralocalized time-series model presented in [33], are devised, featuring online-adjusted structures to enhance flexibility. In addition, some neural networks (NNs) are employed to describe motor behavior, including artificial neural networks (ANNs) in [34] and recurrent neural networks (RNNs) in [35]. However, large-scale implementations are hampered by the significant computational burdens and theoretical upper bounds of accuracy in NNs.

This article offers a comprehensive overview of the fundamental implementations of major data-driven models in MFPC for motor drives. The classification diagram is shown in Fig. 4. The various model structures, implementation types, and their adaptabilities in representing the motor system are analyzed in detail. Given the vastness of the field, not all research activities can be mentioned, but the authors strive to encapsulate the major advancements of the past several years. The unique contributions of this article include: a fresh perspective on MFPC from the predictive control theory, a novel classification of MFPCs based on data-driven model structures, a comprehensive summary of MFPC research, which fills gaps in the existing literature, and the challenges faced and future developments are delved deeply, presenting insights and perspectives.

II. Basic Implementations of MBPC

When it comes to motor drives, MPC is primarily categorized into three distinct types: predictive current control (PCC), predictive torque control (PTC), and predictive speed control (PSC), according to the primary objective of the system. Therefore, there are three main categories of MPC on motor drives: prediction models (MBPC and MFPC), implementation methods (FCS-type and CCS-type), and control objectives (PCC, PSC, and PTC). To simplify the discussion, the following implementations are introduced based on the PCC strategy in a permanent-magnet synchronous motor (PMSM) driving system, aiming to realize inner loop current control, and the other strategies and motor types have similar processes.

A. FCS-Type MBPC Implementation

The physical model of the PMSM can be expressed as the following functions of stator voltage u_{sx}:

$$\begin{cases} u_{sd} = R_s i_{sd} + L_{sd}\frac{\mathrm{d}i_{sd}}{\mathrm{d}t} - L_{sq}\omega_r i_{sq} \\ u_{sq} = R_s i_{sq} + L_{sq}\frac{\mathrm{d}i_{sq}}{\mathrm{d}t} + L_{sd}\omega_r i_{sd} + \omega_r \psi_m \end{cases} \tag{1}$$

where R_s is the stator resistance, L_{sx} is the stator inductance, in which the subscripts x reflect the variable components of d or q, ψ_m is the magnet flux linkage, i_{sx} is the stator current, and ω_r is the electrical angular velocity.

Based on the sampling period T_s, the model can be discretized by the forward Euler algorithm to predict the state variables to the next sampling period

$$\begin{cases} i_{sd}(k+1) = (1-\frac{R_s T_s}{L_{sd}})i_{sd}(k) + \frac{L_{sq}}{L_{sd}}T_s\omega_r i_{sq}(k) + \frac{T_s}{L_{sd}}u_{sd} \\ i_{sq}(k+1) = \\ (1-\frac{R_s T_s}{L_{sq}})i_{sq}(k) - T_s\omega_r i_{sd}(k) - \frac{L_{sd}}{L_{sq}}\psi_m\omega_r i_{sd}(k) + \frac{T_s}{L_{sq}}u_{sq} \end{cases} \tag{2}$$

where $i_{sd}(k)$ and $i_{sq}(k)$ are the discrete-time stator currents at the kth sampling period. When parameter mismatches occur, additional error terms, including ΔR_s, ΔL_{sx}, and $\Delta\psi_m$, are introduced into the model, and these error terms result in extra prediction errors for future currents

$$\begin{cases} \Delta i_{sd}(k+1) = \frac{R_s\Delta L_{sd} - L_{sd}\Delta R_s}{L_{sd}(L_{sd}+\Delta L_{sd})}T_s i_{sd}(k) + \\ \frac{\Delta L_{sq}L_{sd} - \Delta L_{sd}L_{sq}}{L_{sd}(L_{sd}+\Delta L_{sd})}T_s\omega_r i_{sq}(k) + \frac{\Delta L_{sd}T_s}{L_{sd}(L_{sd}+\Delta L_{sd})}u_{sd} \\ \Delta i_{sq}(k+1) = \frac{R_s\Delta L_{sq} - L_{sq}\Delta R_s}{L_{sq}(L_{sq}+\Delta L_{sq})}T_s i_{sq}(k) - \\ \frac{L_{sq}(\psi_m\Delta L_{sd} + \Delta\psi_m L_{sd} + \Delta\psi_m\Delta L_{sd})}{L_{sq}(L_{sq}+\Delta L_{sq})}\omega_r i_{sd}(k) + \\ \frac{L_{sd}\psi_m\Delta L_{sq}}{L_{sq}(L_{sq}+\Delta L_{sq})}\omega_r i_{sd}(k) + \frac{\Delta L_{sq}T_s}{L_{sq}(L_{sq}+\Delta L_{sq})}u_{sq}. \end{cases} \tag{3}$$

According to the primary objective of the PCC strategy, its cost function is usually designed as

$$J = (i_{sd}(k+1) - i_{sd}^*(k+1))^2 + \mu(i_{sq}(k+1) - i_{sq}^*(k+1))^2 \tag{4}$$

where μ is the weighting factor, and $i_{sd}^*(k+1)$ and $i_{sq}^*(k+1)$ are the future current references on the d- or q-axes.

In the FCS-type, all candidate vectors will be substituted into the cost function in turn. The vector that obtains the minimum cost function value can realize the minimum target error, that is, this vector can be regarded as the optimal vector for the driver's operation [2]. To accommodate complex prediction models or long prediction horizons, incorporating advanced cost function minimization methods can be beneficial. Some options to consider include the preliminary election method in [36], sphere decoding in [37], and k-best sphere decoding in [38]. These methods have the potential to decrease the computational load and free up more processor resources.

B. CCS-Type MBPC Implementation

To realize the CCS-type, a group of control functions is required to generate modulation waves. Taking partial derivatives of stator voltage components in the cost function, and making their results zero, the control function is expressed as follows based on the discrete-time model of motors:

$$\begin{cases} \frac{\partial J}{\partial u_{sd}} = 0 \\ \frac{\partial J}{\partial u_{sq}} = 0 \end{cases} \Rightarrow \begin{cases} u_{sd} = (R_s - \frac{L_{sd}}{T_s}) i_{sd}(k+1) - L_{sd} i_{sq}(k+1)\omega_r \\ u_{sq} = (R_s - \frac{L_{sq}}{T_s}) i_{sq}(k+1) + L_{sq} i_{sd}(k+1)\omega_r \\ \qquad + L_{sq}\psi_m \omega_r + \frac{L_{sq}}{T_s} i_{sq}^*(k+1) \end{cases} \tag{5}$$

where the optimal solution is found in each sampling period, and this is a dynamic process that adapts to changing system conditions. A modulation, such as space vector modulation, is required to generate pulses and make the motor drives reach the objectives [39].

C. Robustness Analysis

No matter under the FCS or CCS-type conditions, according to (1) and (5), they both contain some time-varying physical parameters, such as stator resistance R_s, stator inductance L_{sx}, and magnet flux linkage ψ_m. These parameters are the basic reason for the weak robustness in MBPC.

Under the conditions of a changing load torque from 0 to 11.5 N·m and a speed from 1000 to 1500 r/min with a fixed sampling period of 62.5 μs, Fig. 5 shows the experimental waveforms obtained by CCS-type MBPC with and without a group of parameter mismatches, operated on all physical parameters and their components on the dq-frame. As shown in Fig. 5(a) and (b), this strategy can stably operate following the reference and resisting the disturbances. Due to the limited bandwidth of the outer loop, the dynamics do not have significant improvements in the experiments. Selecting the parameter mismatching condition for the experiments as follows: resistance is set to 0.5 times its rated value, d- and q-axes inductances are both set to 2 times their rated values, and permanent-magnet flux is set to 0.5 times its rated value. As shown in Fig. 5(c) and (d), when the parameter mismatches are acting on the system, the current quality has

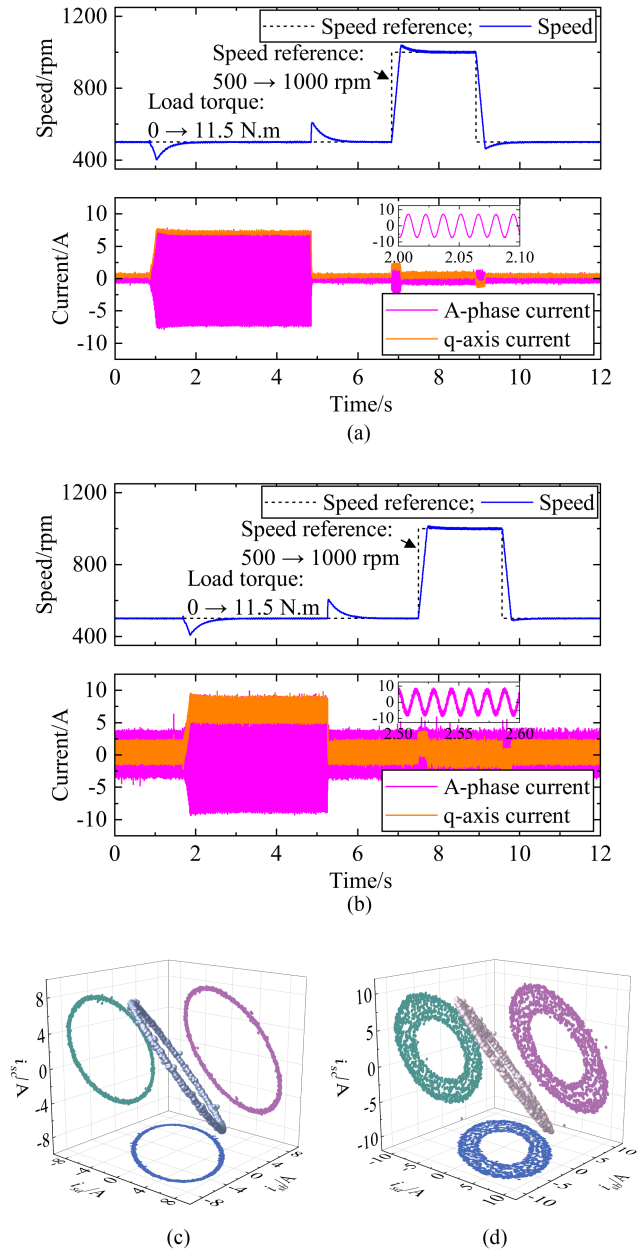

Fig. 5. Experimental waveforms of CCS-type MBPC. (a) Waveforms without parameter mismatches. (b) Waveforms with parameter mismatches. (c) Current distributions without parameter mismatches. (d) Current distributions with parameter mismatches.

an obvious negative influence, due to the combined effects of multiple parameter mismatches, particularly inductance errors, validating the aforementioned weak robustness.

Regarding the FCS-type and CCS-type MBPCs, the only difference lies in the process of cost function minimization. Since the prediction model used in the prediction process is the same for both CCS and FCS-type MBPCs, the prediction errors in (3) are inserted into the prediction values for both methods. A similar trend of change could be observed in the case of FCS-type MBPC, indicating that both methods are affected by parameter mismatches in a similar manner.

D. Simple Extension of Other Control Types and Motor Drives

The speed and torque controllers are also crucial in the general motor driving system. For example, in the case of PSC for the motor drives, the physical model is extended as

$$\frac{\mathrm{d}\boldsymbol{x}}{\mathrm{d}t} = h(\boldsymbol{x}, \boldsymbol{u}) \tag{6}$$

where

$$\boldsymbol{x} = [i_{sd}, i_{sq}, \omega_r]^T$$
$$\boldsymbol{u} = [u_{sd}, u_{sq}]^T$$
$$h(\boldsymbol{x}, \boldsymbol{u}) = \begin{bmatrix} -\frac{R_s}{L_{sd}} i_{sd} + \frac{L_{sq}}{L_{sd}} \omega_r i_{sq} + \frac{1}{L_{sd}} u_{sd} \\ -\frac{R_s}{L_{sq}} i_{sq} - \frac{L_{sd}}{L_{sq}} \omega_r i_{sd} - \frac{\psi_m}{L_{sq}} \omega_r + \frac{1}{L_{sq}} u_{sq} \\ \frac{1.5p^2}{J}(\psi_m i_{sq} + (L_{sd} - L_{sq}) i_{sd} i_{sq}) - \frac{B}{J}\omega_r \end{bmatrix} \tag{7}$$

in which B is the friction coefficient, J is the rotor inertia, and p is the number of pole pairs.

This model reveals that certain parameters for the speed controller, such as B and J in (7), are more challenging to acquire. Although the following analyses are specifically conducted based on PCC, the results can be extended for applications in PSC and PTC, areas where MFPC also good at [40].

Furthermore, the review work is not limited to the three-phase frame. In addition to typical motor types, some multiphase motor drives and special motors are also taken into consideration. However, parameters for harmonic subspaces in multiphase motors, such as xy leakage inductance L_{ls} in (8), are difficult to obtain accurately. Nevertheless, MFPC can also be effectively applied in these scenarios.

$$\begin{bmatrix} u_{s\alpha} \\ u_{s\beta} \\ u_{sx} \\ u_{sy} \end{bmatrix} = R_s[I_{4\times4}] \begin{bmatrix} i_{s\alpha} \\ i_{s\beta} \\ i_{sx} \\ i_{sy} \end{bmatrix} + \begin{bmatrix} L_{\alpha\alpha} & L_{\alpha\beta} & 0 & 0 \\ L_{\beta\alpha} & L_{\beta\beta} & 0 & 0 \\ 0 & 0 & L_{ls} & 0 \\ 0 & 0 & 0 & L_{ls} \end{bmatrix} \begin{bmatrix} \dot{i}_{s\alpha} \\ \dot{i}_{s\beta} \\ \dot{i}_{sx} \\ \dot{i}_{sy} \end{bmatrix} + \psi_m \begin{bmatrix} \cos(\theta_r) \\ \sin(\theta_r) \\ 0 \\ 0 \end{bmatrix}. \tag{8}$$

III. Data Models Based on Direct Data

According to the implemental principle of MFPC in Fig. 2, it is apparent that the physical model has been superseded by a data-driven model. For FCS-type predictive control in the aforementioned PMSM drives, this model requires capturing the intricate causal relationship between voltage and current, and employing a cost function to identify the optimal control vector. Besides, the CCS-type emphasizes the causal link from current to voltage, leveraging a control function powered by an intersection algorithm to generate control signals. Ultimately, the success of achieving the desired control objectives lies in the model adaptability, relating to the model structure and its estimation algorithm.

This section primarily discusses the ultralocal model, time-series model, and subspace model. In addition, there are other data-driven models within this category that can be utilized for motor drive systems, such as the incremental voltage prediction model in [41], the nonparametric prediction model in [29], and Koopman operators in [42].

A. Ultralocal Model (Hyperlocal Model)

1) Model Structure: For an n-order SISO system, it can be described as the following full-form ultralocal in theory:

$$\iota_0 \frac{\mathrm{d}^n \boldsymbol{x}}{\mathrm{d}t^n} + \iota_1 \frac{\mathrm{d}^{n-1} \boldsymbol{x}}{\mathrm{d}t^{n-1}} + \cdots + \iota_{n-1} \frac{\mathrm{d}\boldsymbol{x}}{\mathrm{d}t} + \iota_n \boldsymbol{x} + \boldsymbol{F} = \gamma_0 \frac{\mathrm{d}^m \boldsymbol{u}}{\mathrm{d}t^m} + \gamma_1 \frac{\mathrm{d}^{m-1} \boldsymbol{u}}{\mathrm{d}t^{m-1}} + \cdots + \gamma_{m-1} \frac{\mathrm{d}\boldsymbol{u}}{\mathrm{d}t} + \gamma_m \boldsymbol{u} \tag{9}$$

where $\boldsymbol{x}$ ($= \boldsymbol{i}_s = [i_{sd}, i_{sq}]^T$) is the state signal, which equals to the output signal of $\boldsymbol{y}$ in the models, $\boldsymbol{u}$ ($= \boldsymbol{u}_s = [u_{sd}, u_{sq}]^T$) is the input signal, and $\boldsymbol{F} = [F_d, F_q]^T$ is the lumped variable summarizing the other unknown terms of the plant.

For the motor drives, the ultralocal model requires real-time implementation. This model is mainly simplified into three distinct forms: basic form, advanced form, and affine form, listed as follows:

$$\frac{\mathrm{d}^n \boldsymbol{x}}{\mathrm{d}t^n} = \gamma \boldsymbol{u} + \boldsymbol{F} \tag{10}$$

$$\frac{\mathrm{d}^n \boldsymbol{x}}{\mathrm{d}t^n} = \gamma \boldsymbol{u} + \iota \boldsymbol{x} + \boldsymbol{F} \tag{11}$$

$$\frac{\mathrm{d}^n \boldsymbol{\varepsilon}}{\mathrm{d}t^n} = \gamma \boldsymbol{u} + \boldsymbol{F}_0 + \boldsymbol{F}_1 \boldsymbol{\varepsilon} + \boldsymbol{\varepsilon}^T \boldsymbol{F}_2 \boldsymbol{\varepsilon} + \cdots \tag{12}$$

where γ is the input gain, ι is the state gain, $\boldsymbol{F}_0, \boldsymbol{F}_1, \boldsymbol{F}_2, \cdots$ are the affine operators, and $\boldsymbol{\varepsilon}$ is the normalized tracking error of input signals. Unlike the basic and advanced forms, the affine-form tries to incorporate more components of the state variable into a single, comprehensive model.

2) FCS-Type Implementation: To implement MFPC utilizing ultralocal approaches in the FCS-type, the model must be established first. For the nonzero input gain γ, this value directly impacts the robustness and steady-state performance of the system [43]. There are two types of calculation methods: offline and online [44], [45]. Offline schemes are commonly adopted due to their simplicity, converting the physical model into an ultralocal form and treating the term related to the input signal as the gain value [46]. Although the input gain may encompass some physical parameters, in practice, it is considered a nonphysical constant, and the time-varying parameters and their impacts are not factored into this value [47].

Regarding the lumped variable of $\boldsymbol{F}$, it can be estimated using algebraic algorithms or observers. The former primarily includes algebraic parameter identification [48], [49], signal differences [50], and the RLS algorithm [51]. The latter has been extensively studied in recent years, such as ESO in [52], SMO in [12], Luenberger observer in [53], and nonlinear observer in [54]. These observers treat the negative impacts of parameter mismatches as disturbances and compensate for them accordingly. Of course, there are also advanced observers, such as linear disturbance observers [55] and harmonic injection ESOs [56],

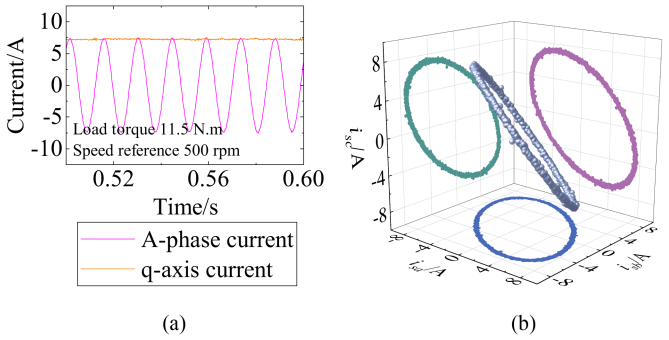

Fig. 6. Experimental results of CCS-type MFPC using ultralocal with parameter mismatches. (a) Experimental waveforms. (b) Current distributions.

which aim to achieve better compensation results and control performance.

During the prediction process, when an observer is employed for estimation, predicted variables are derived using discrete-time formulas and substituted into the cost function to find the optimal vector. The consideration of time shift can be utilized to realize the prediction process in algebraic algorithms.

3) CCS-Type Implementation: In the CCS-type systems, once the updated model is implemented, MFPC utilizing ultralocal techniques often requires employing the intelligent proportional-integral-derivative (iPIDs) structure in [57] and [58] to generate control functions

$$\boldsymbol{u}_s = -\frac{1}{\gamma}\left(\boldsymbol{F} - \frac{\mathrm{d}^2\boldsymbol{i}_s^*}{\mathrm{d}t^2} + k_p\boldsymbol{\varepsilon} + k_i\int\boldsymbol{\varepsilon} + k_d\frac{\mathrm{d}\boldsymbol{\varepsilon}}{\mathrm{d}t}\right) \tag{13}$$

where k_p, k_i, and k_d are the usual tuning gains. For general motor driving systems, an intelligent proportional (iP) structure, coupled with modulation techniques, is to produce suitable control signals without any negative impacts on the dynamics of the control strategy, preserving the core advantage of MPC due to the infinite bandwidth of the iP structure [47], [59]. However, when the integral term is included in the iPID structure, the bandwidth may be affected if no special process such as the switched MFPC in [32] is used, potentially compromising the dynamic performance.

Since MFPCs do not include any physical parameters in the updating and prediction processes, their robustness is validated by the training data of the initial data-driven model (i.e., ultralocal in this section) obtained by the MBPC with parameter mismatches, where these mismatches are consistent with the conditions outlined in Fig. 4(b). For the CCS-type MFPC using ultralocal, the experimental waveforms and the current distributions are shown in Fig. 6, within the steady state. As shown in the figures, the current quality almost unaffected by the mismatches, and effectively enhance the robustness.

4) Challenges of Implementation: There are two significant challenges in implementation: input gain selection and iPID gain selection.

Taking the driving system in Section II as an example, in the CCS-type, the experimental waveforms of MFPC using ultralocal and the continuous Fourier analysis results are shown

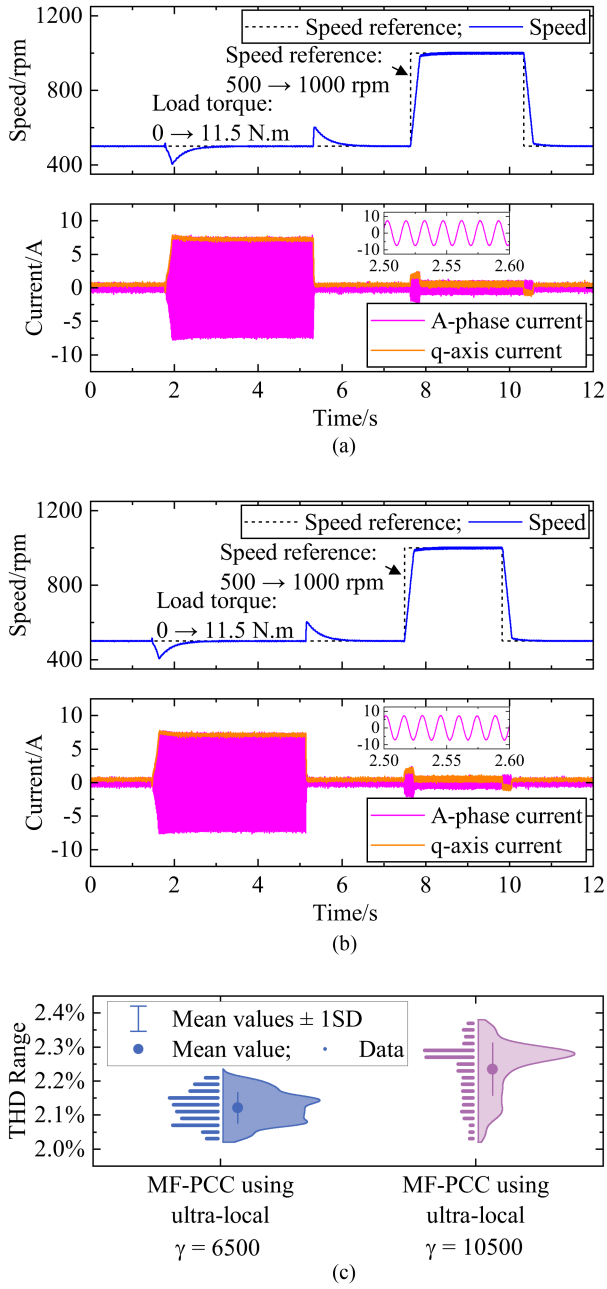

Fig. 7. Experimental waveforms of CCS-type MFPC using ultralocal (ω_r^* of 500 r/min, T_L of 11.5 N · m). (a) Waveforms with an input gain of 6500. (b) Waveforms with an input gain of 10500. (c) Continuous Fourier analysis results.

in Fig. 7. They show that the input gain has an obvious influence on the objective quality. Furthermore, Fig. 8 shows that the optimal value of the input gain changes under different operating conditions, such as different load torque and speed references. Therefore, an adaptive approach for input gain is necessary for MFPC to enhance model adaptability and prediction accuracy.

If the iP structure is employed in the CCS-type system, only one gain is required, which can be readily determined through repetitive experimental outcomes. However, to achieve superior tracking errors and dynamics comprehensively, an iPID or a

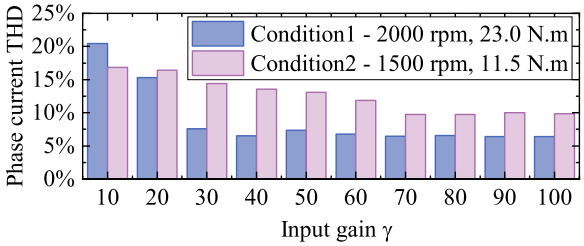

Fig. 8. Objective quality with different input gains and operating conditions by MFPC using ultralocal in experiments.

more intricate structure is necessary, such as the switching ultralocal based on an exponential-like function in [32]. These structures necessitate the tuning of additional gains, and the complexity of the selection process is challenging to implement within the control strategy.

B. Time-Series Model

1) Model Structure: The fundamental structure of the time-series model is ARX, which is expressed as follows [23]:

$$G_x(z^{-1})x_j(k) = \sum_{i=1}^{l_u} G_{u,i}(z^{-1})\boldsymbol{u}(k) \tag{14}$$

in which

$$\begin{cases} G_x(z^{-1}) = \alpha_0 + \alpha_1 z^{-1} + \cdots + \alpha_m z^{-m} \\ G_{u,i}(z^{-1}) = \beta_{0,i} + \beta_{1,i} z^{-1} + \cdots + \beta_{n,i} z^{-n} \end{cases} \tag{15}$$

where x_j is an element of $\boldsymbol{x}$, l_u and l_x are the length of $\boldsymbol{u}$ and $\boldsymbol{x}$, respectively, α_m and $\beta_{n,i}$ are the model coefficients, and m and n are the model orders (or orders for the polynomials). α_0 is always selected as 1 to ensure the causality of the plant.

For the ARMA model, the input signal has an extra requirement of

$$\begin{cases} E(u_i(k)) = 0, E(u_i(k_1)u_i(k_2)) = 0 (i \in 1, \ldots, l_u) \\ E(u_i(k_1)x_j(k_2)) = 0 (\forall k_1 < k_2, j \in 1, \ldots, l_x) \\ \alpha_0 \neq 0, \beta_{0,i} \neq 0 \end{cases} \tag{16}$$

where $E(.)$ is the expected value of the variable. To fulfill this requirement, the state variables can be selected as ε in MFPC using ARMA. For simplicity in modeling, this model can be reduced to AR(1) and MA(1), respectively.

2) FCS-Type Implementation: The suitable coefficients of the model are crucial for achieving good adaptability in the time-series model. To estimate these coefficients online, the RLS algorithm is typically employed based on grouped sampled data and coefficients [60]. However, the relatively slow convergence rate of the RLS algorithm poses a challenge to its adaptability. A normalized least-mean-square (NLMS) algorithm is introduced to reduce computational burdens and enhance the convergence rate. In addition, a recursive gradient correction (RGC) algorithm is designed specifically for the ARMA model, aiming to further minimize the computational burden.

During the establishment and updating process of the time-series model, the following time-shift consideration is always employed to predict the state variables to a future sampling period, confirming the preset prediction horizon

$$\begin{aligned} &\alpha_m(k+1) \approx \alpha_m(k), \beta_{n,i}(k+1) \approx \beta_{n,i}(k) \\ &\Rightarrow x_j(k+1) = \alpha_0 x_j(k) + \cdots + \alpha_m x_j(k-m+1) + \\ &\sum_{i=1}^{l_u} (\beta_{0,i} u_i(k+1) + \cdots + \beta_{n,i} u_i(k-n+1)) \end{aligned} \tag{17}$$

in which $u_i(k+1)$ is the candidate vectors, and the future $x_j(k+1)$ is adopted to join the cost function calculation.

3) CCS-Type Implementation: There are two approaches to realizing MFPC using time series in the CCS-type: the reverse causality model and the ultralocalization model. The former involves swapping the positions of state signals and input signals in (14). Within the context of time-shift considerations, $u_i(k+1)$ is substituted with its future references obtained through the Lagrange algorithm. The latter approach adjusts the model structure in (14) to resemble the ultralocal model in (10) after the estimation process is complete. The iP structure in (13) can then be utilized to generate control signals, where the proportional gain is selected using the particle swarm optimization (PSO) algorithm in an auxiliary processor [33]. One advantage of the latter approach is that both γ and $\boldsymbol{F}$ in (10) are automatically calculated at the same time by the RLS algorithm, thereby indirectly addressing the challenge of the MFPC using the ultralocal model [61].

4) Challenges of Implementation: Two significant implementation challenges lie in the low converging rate of the estimation algorithm and the selection of orders under limited processor resources, respectively.

For the former, under parameter mismatches, Fig. 9 presents the experimental waveforms for MFPC using ARX of [$n = 2$, $m = 2$], including the converging process of some coefficients within two transient-states. As shown in the figures, on the one side, the enhanced robustness is validated effectively. On the other side, these coefficients exhibit a comparatively slower convergence rate than the currents, indicative of reduced model adaptability during the convergence process. Although the accelerated estimation algorithms of NLMS and RGC have better convergence rates, these algorithms still necessitate an improvement to fully prevent possible instability within the transient states.

For the latter, Fig. 10 shows the experimental waveforms of MFPC using ARXs with different orders, and their accumulated objective errors. As shown in the figures, different orders are applicable to changing operating states. During two operating states within continuous 16 000 sampling points in simulation, Fig. 11 further shows the accumulated objective errors of ARXs with different orders in a wider range, showing the requirements for orders vary under different operating conditions, necessitating an adaptive approach to order selection. However, the computational times of these strategies are tested in Fig. 12 in the CCS and FCS-types, respectively, in which the program of the

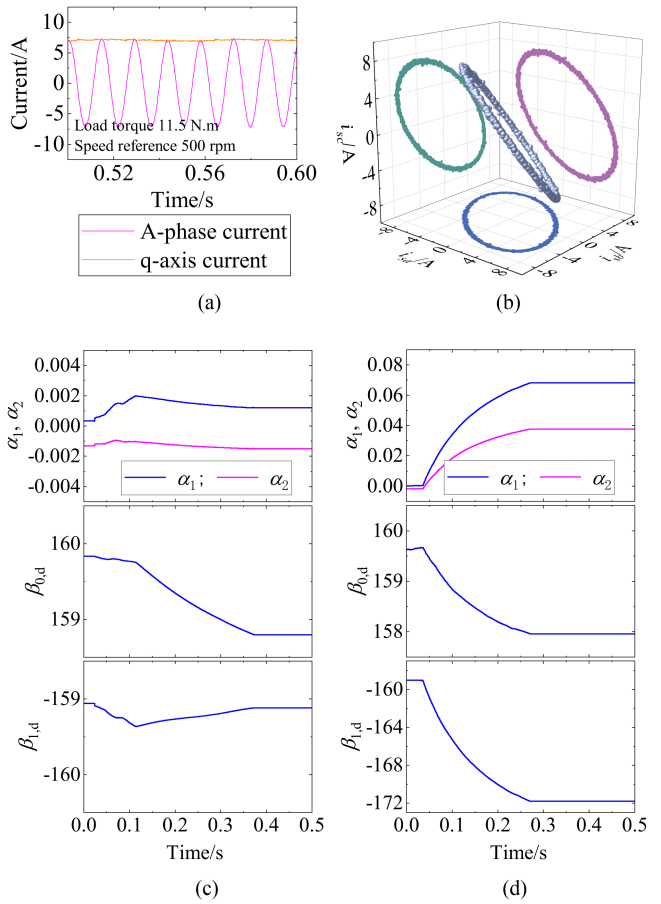

Fig. 9. Experimental results of CCS-type MFPC using ARX of $[n = 2, m = 2]$ with parameter mismatches. (a) Experimental waveforms. (b) Current distributions. (c) Converging process of model coefficients within the changing load torque from 0 to 11.5 N· m. (d) Converging process of model coefficients for changing reference from 500 to 1000 r/min.

FCS-type result is fine-processed to reduce the computational burdens as far as possible. Despite being affected by randomness, the results show that an upper bound of orders should be carefully considered in the implementation of MFPC using time series for motor drives, to prevent overrun errors. Furthermore, this strategy is more suitable in the CCS-type since the FCS-type implementation requires repetitive estimation processes based on different candidate vectors, generating rigorous requirements for the processor resources.

C. Subspace Model

To derive a subspace model, the collection of state signals and input signals is structured using Hankel matrices, denoted as $\mathscr{H}(\boldsymbol{u}^c)$ and $\mathscr{H}(\boldsymbol{x}^c)$, respectively, based on the prediction horizon N. These matrices are partitioned into past and future sub-blocks, i.e., $[\boldsymbol{U}_p, \boldsymbol{U}_f]^T = \mathscr{H}(\boldsymbol{u}^c)$ and $[\boldsymbol{X}_p, \boldsymbol{X}_f]^T = \mathscr{H}(\boldsymbol{x}^c)$, which can be solved using the least-squares algorithm. The subspace model is then constructed as an ARX predictor through singular value thresholding [62]

$$\boldsymbol{x}_f = \boldsymbol{P}_w(\boldsymbol{u}_p, \boldsymbol{x}_p)^T + \boldsymbol{P}_u \boldsymbol{u}_f \tag{18}$$

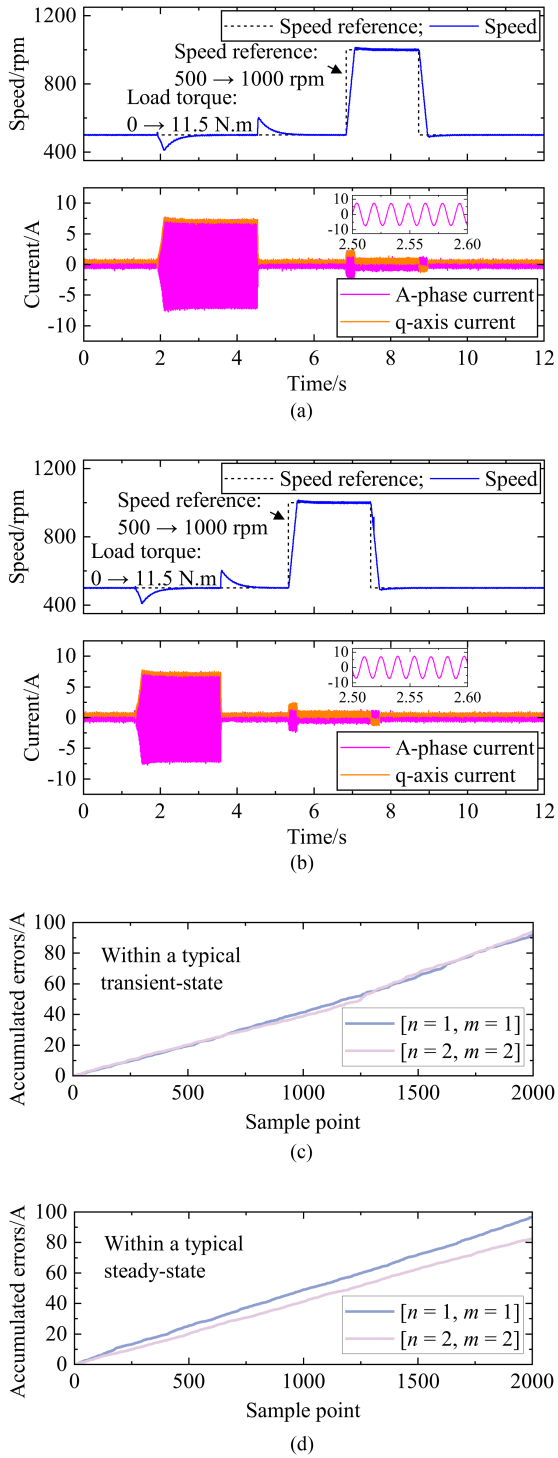

Fig. 10. Experimental results of CCS-type MFPC using ARX. (a) ARX of $[n = 1, m = 1]$. (b) ARX of $[n = 2, m = 2]$. (c) Accumulated errors within a typical transient state. (d) Accumulated errors within a typical steady state.

where $\boldsymbol{u}_p$ and $\boldsymbol{x}_p$ are the past input and state signals, and $\boldsymbol{u}_f$ and $\boldsymbol{x}_f$ are the future input and state signals, respectively. $\boldsymbol{P}_w$ and $\boldsymbol{P}_u$ involve past and future elements of Hankel matrices, computed by solving the least-squares problem [63]. When a short prediction horizon is set in MFPC, the subspace

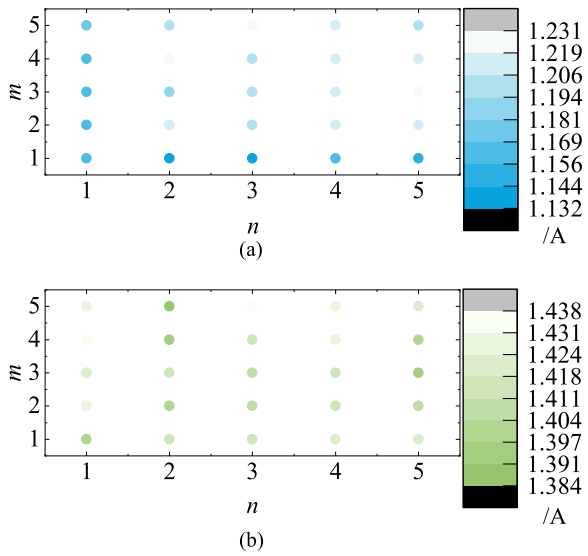

Fig. 11. Accumulated current errors with different orders in MFPC using time series in simulations. (a) Operating state 1. (b) Operating state 2.

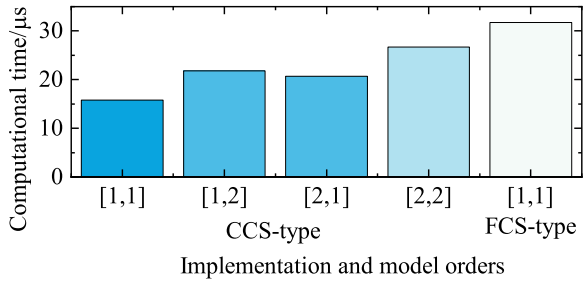

Fig. 12. Computational times with different implementations and model orders.

model can be approximately regarded as ARX, where all elements in the matrices are considered as discrete-time signals. Therefore, their implementations and challenges are largely analogous.

IV. Data Models Based on Data Gradients

For the predictive control based on direct data, according to the quadratic programming (QP)-type cost functions in the control theory of MPC, the optimal control function can be transformed into a proportional form, which fails to fully eliminate static errors. If an incremental model is employed in the predictive control, an integral calculation of $\boldsymbol{u}(k) = \sum_i \Delta u_{sx}(i)$ is incorporated into the control functions to mitigate static errors. Hence, suitable data-driven models grounded in data gradients are sought in MFPC to enhance model adaptability.

This section mainly focuses on the LUT and dynamic-linearization model. In addition, within this category, there are also several other data-driven models that can be applied to motor drive systems. These include the GUM in [30], the incremental-type ultralocal model in [64], the self-commissioning model in [65], and various models based on variable slopes in [66] and [67].

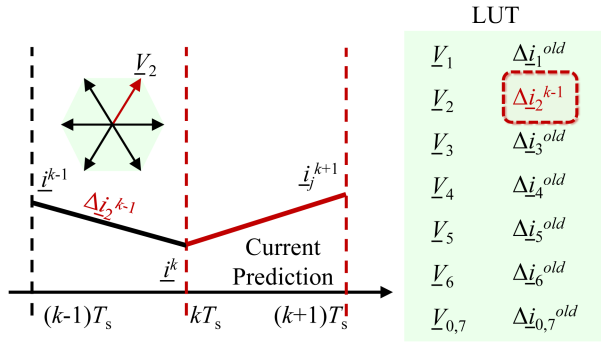

Fig. 13. Basic principle of LUT implementation.

A. Lookup Table (LUT)

1) Model Structure and FCS-Type Implementation: In the MFPC using the LUT, all gradients of $\boldsymbol{x}$ by candidate vectors are summarized in a table to approximately derive the future $\boldsymbol{x}$ from the measured data and their corresponding gradients. This table at the (k-1)th sampling period is viewed as a representation of future results and substituted into the cost function to identify the optimal solution. As illustrated in Fig. 13, taking the vector V_2 as an example, the element is updated whenever this vector is selected as the optimal choice, maintaining the adaptability of the LUT [68].

Fig. 14 shows that the experimental waveforms of the FCS-type MFPC using the LUT, in which Fig. 14(b) is implemented at $2f_{\text{sample}} = f_{\text{updating}}$, to forcibly set some extra continuous stagnations (i.e., the stagnation appears within two intervals continuously at least). The current quality has an obvious decrement compared with the strategies in the CCS-type. The reason is that excepting the negative impacts on all harmonic content increments caused by the variable switching frequency in FCS-type, the stagnation effect is also an important influencing factor due to the modeled data gradients, and this challenge will be discussed in the following section in detail.

2) Challenges of Implementation: The stagnation effect represents a significant challenge for the MFPC using the LUT. Here is the definition for the stagnation and its effects [69]: The stagnation arises due to limitations in low updating frequency, causing the data to remain static across continuous sampling periods. This restricts the model's adaptability, impeding its ability to comprehensively capture the plant's operating states. Specifically for LUT-based MFPC, its stagnation is due to the fact that only the optimal elements are updated during each sampling period, while other elements are not operated upon. Consequently, the stagnation effect adversely affects the quality of the control strategy.

Two types of antistagnation approaches address the stagnation effect: the direct and the indirect methods. The former tackles the issue by enhancing the updating frequency, at the cost of a higher possibility of suboptimal selections and additional prediction errors. For instance, in the method in [70], if a base voltage is not applied for a predefined time window, the voltage vector is forcedly set as the next voltage reference. In [71], two contiguous measured current gradients due to the applied voltage vectors are

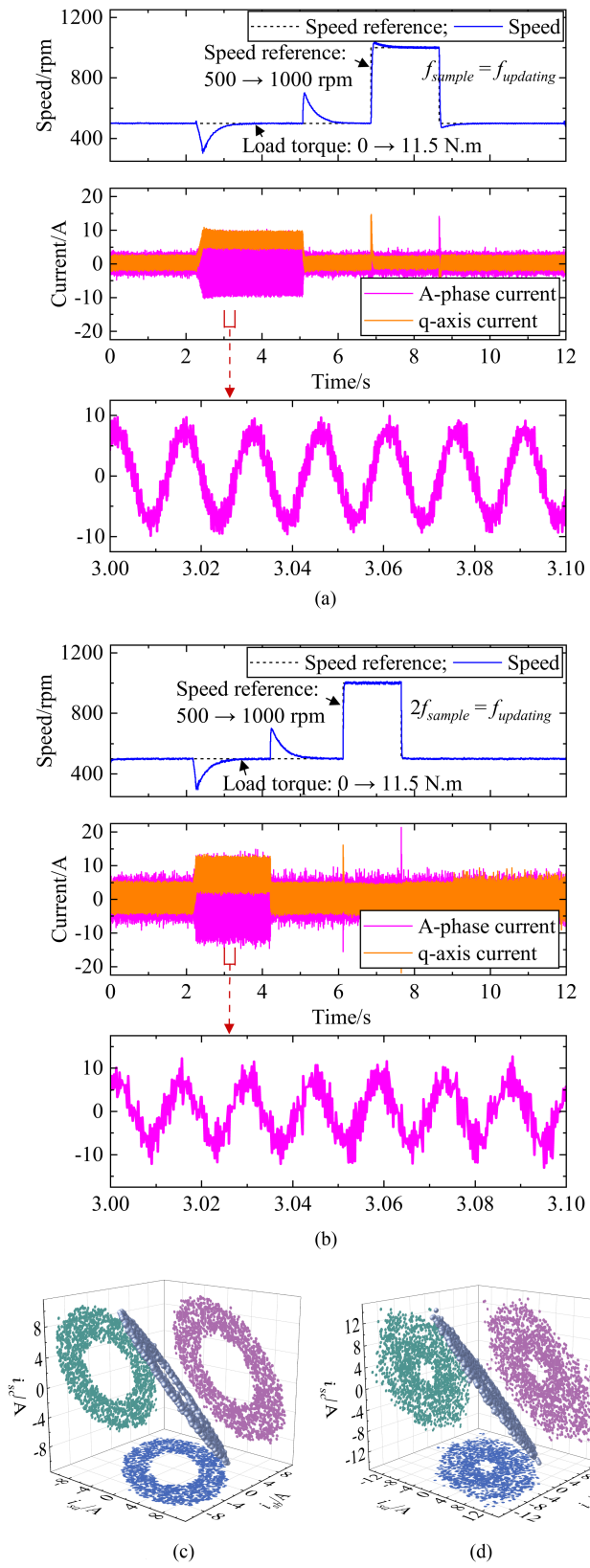

Fig. 14. Experimental results of FCS-type MFPC using the LUT. (a) Waveforms with $f_{\text{sample}} = f_{\text{updating}}$. (b) Waveforms with $2f_{\text{sample}} = f_{\text{updating}}$. (c) Current distributions with $f_{\text{sample}} = f_{\text{updating}}$. (d) Current distributions with $2f_{\text{sample}} = f_{\text{updating}}$.

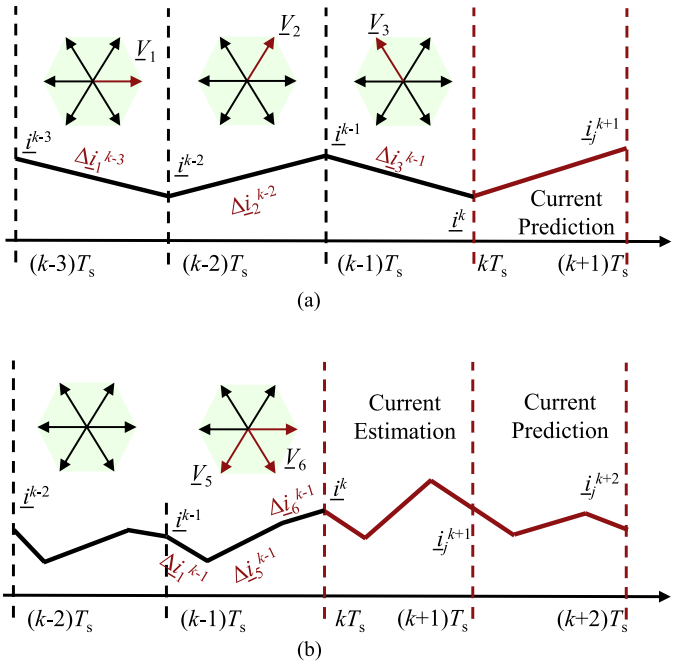

Fig. 15. Sketch diagrams of some improved LUT implementations. (a) Method in [71]. (b) Method in [73].

used to estimate the current gradients for all candidate voltage vectors, as shown in Fig. 15(a). This keeps the current gradient information up to date and addresses the stagnation problem. The latter, the indirect method, focuses on reconstructing LUTs indirectly. The methodology in [26] updates LUTs based on mathematical relationships between inverter input voltages. By knowing the last three current variations, it enables an approximate update of other LUT elements. In [72], a real-time update frequency is implemented to refresh the current difference upon detection, thus preventing stagnation. Furthermore, an extended LUT updating mechanism is introduced in [27] to generate synthetic vectors composed of double vectors and stored in the tables. This mechanism is advanced to synthetic triple vectors in [73] to further mitigate the adverse effects of stagnations, as shown in Fig. 15(b). To eliminate the stagnation effect entirely, an antistagnation mechanism with enhanced reliability and performance is presented in [74], effectively improving prediction accuracy by utilizing a pair of antiphase vectors and corresponding current variations, avoiding update stagnation. Moreover, the predicted slopes of current vector components are utilized in the prediction and voltage vector selection processes in [75]. Notably, this methodology does not employ LUTs for inverter switching configurations, which does not face the stagnation effect.

Two typical anti-stagnation methods are selected, one direct (from [71]) and one indirect (from [27]), as examples to demonstrate their effectiveness. These two methods are applied to the typical LUT-based MFPC under identical conditions. Both direct and indirect methods are able to mitigate the negative effects of stagnation, and their continuous Fourier results are illustrated in Fig. 16. The direct method in [71] calculates the remaining

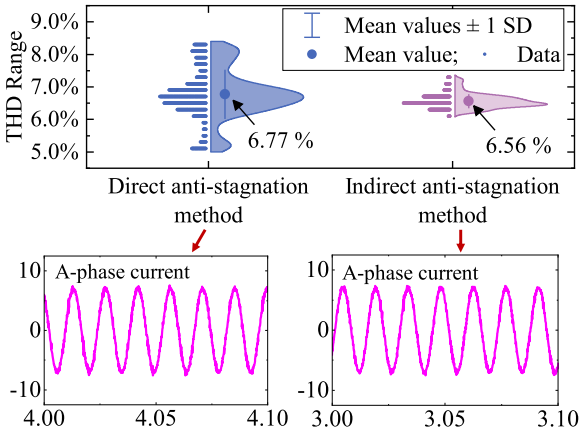

Fig. 16. Comparison of continuous Fourier results for LUT-based MFPC with different antistagnation methods.

current gradient based on the updated gradient of vectors applied in the past three cycles. However, if these vectors remain the same for three consecutive cycles, the method may become ineffective, limiting the optimization of current quality. Consequently, this method brings in some extra prediction errors, resulting in a larger total harmonic distortion range.

In addition, as a supplement to the stagnation effect, previous research has primarily focused on LUT-based MFPC, both direct and indirect methods. However, other MFPCs also be affected by stagnation, albeit to varying degrees [69]. Specifically, the single model structure (data gradient) that use data gradients to update results, such as LUT and GUM, may experience static process within continuous intervals, leading to estimation errors and compromising system stability. In contrast, the single model structure (direct data) that use direct data updates, such as ULM and time series, continue to update the model even if the sample data are continuously the same, which can be seen as an increase in the control horizon. Therefore, while the single model structure (direct data) does not face the same severe stagnation as the single model structure (data gradient), it still experiences some impact on their operating performance.

B. Dynamic-Linearization Model

Dynamic linearization is an earlier model within MFPC and model-free adaptive predictive control with adjustable models, recently always employed to describe large-scale systems. Based on the pseudopartial derivative (PPD) principle, this model primarily characterizes the system in three forms: compact form, partial form, and full form, which are listed as follows [76], [77]

$$\Delta x(k+1) = \phi_c(k)\Delta u(k) \tag{19}$$

$$\Delta x(k+1) = \boldsymbol{\phi}^T_{p,l_u}(k)\Delta \boldsymbol{u}(k) \tag{20}$$

$$\Delta x(k+1) = \boldsymbol{\phi}^T_{f,l_x,l_u}(k)\Delta \boldsymbol{H}_{l_x,l_u}(k) \tag{21}$$

where $\phi_c(k)$, $\boldsymbol{\phi}^T_{p,l_u}(k)$, and $\boldsymbol{\phi}^T_{f,l_x,l_u}(k)$ are PPD time-varying vectors, including all unknown terms of the plant and ensuring

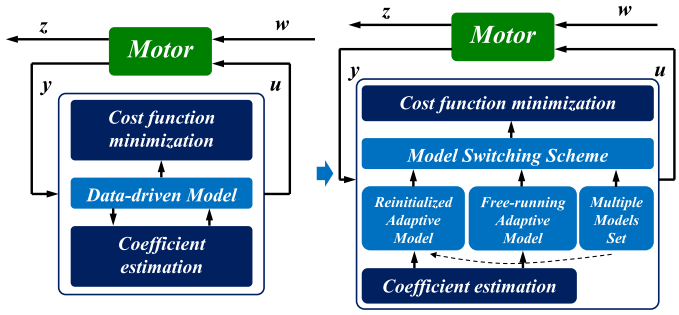

Fig. 17. Sketch diagram of MFPC using full-data multimodels [79].

bounded system at any time within operating process. $\boldsymbol{H}_{l_x,l_u}(k)$ is a sliding window for the input signal. To consider the residual nonlinear uncertainties $\Theta(k)$ of the model, the model is improved as [78]

$$\Delta x(k+1) = \phi_c(k)\Delta u(k) + \Theta(k). \tag{22}$$

Furthermore, as the models are updated based on data gradients, the stagnation effect also impacts the control quality in MFPCs inevitably.

V. Transitional Model Structures (Full-Data Multimodels)

The multimodel approach is an effective method for generating a transitional model in predictive control, considering more operating states of the plant, and its flexibility is at an intermediate level between the single data-driven model mentioned previously and the flexible model in the next section. The implementing key is changed from model estimation to smooth switching for multimodels. However, this idea is difficult to realize in actuality for data-driven, due to the heavy computational burdens in the updating and prediction processes in MFPC.

A typical method is a multimodel switching predictive control in [79] for active fault tolerance of motor drives. As shown in Fig. 17, the data-driven model is divided into three parts: reinitialized adaptive model, free-running adaptive model, and multimodels set. For the multimodels set, there are p^* time-series submodels that describe different operating states of the plant, where the number of p^* submodels is determined by subtraction clustering. The free-running adaptive model with online updating coefficients is established to ensure stability, and the reinitialized adaptive model is used to improve the convergence rate. In addition, a model switching scheme is designed based on the output error, to determine which scheme has the strongest adaptability to the plant property, aiming to update the three parts of the model.

Due to resource constraints and the complexity of implementing multimodels, some simulation results are conducted in Fig. 18, which show the waveforms of speed, q-axis current, and A-phase current, to demonstrate the feasibility and performance. These results demonstrate that the model can successfully track the reference and resist disturbances. Since the initial data are

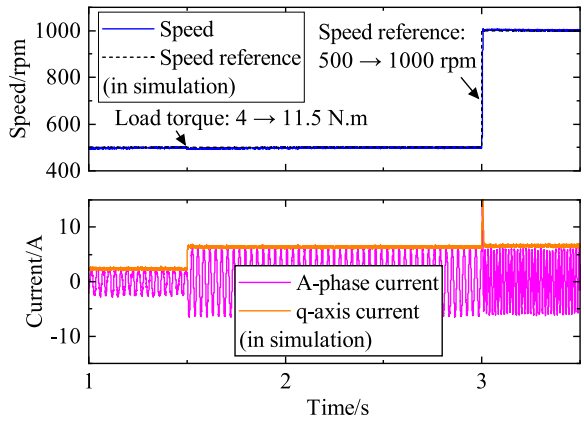

Fig. 18. Simulation results of multimodel-based MFPC.

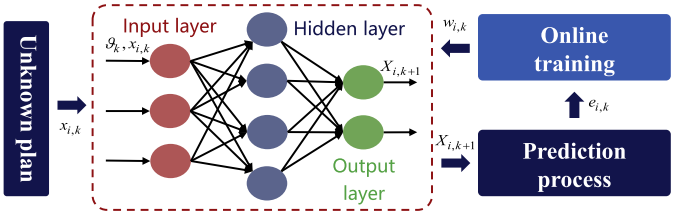

Fig. 19. Sketch diagram of MFPC using neural networks.

generated by the MBPC with parameter mismatches, the robustness of the system is validated. Regarding the feasibility of transitional models, they have potentiality to integrate multiple same data models, different data models, and even data-physical models, enhancing the model's adaptability compared to single-model MFPCs.

VI. Flexible Models Using Neural Networks

Due to the superiorities of NNs including strong nonlinear mapping ability, high adaptability, and good prediction accuracy, this kind of model is valuable in MFPC [80]. Its sketch diagram is shown in Fig. 19. Such as the RNN in [81], this model relies solely on the identification of motor drive signals, disregarding the need for parameter considerations, leading to remarkable dynamics and minimal tracking errors. In addition, an integration-enhanced noise-tolerant zeroing neural network (ZNN) is designed in [82] specifically for robotic arm motors, effectively mitigating the impacts of severe noise. Furthermore, a state-space neural network (ssNN) is introduced in [83] for MFPC, where all weights are optimized via the PSO algorithm, facilitating faster convergence. By leveraging reinforcement learning, MFPC also achieves totally model-free effectively enhancing robustness. Furthermore, combining with the reinforcement learning, the event-driven method offers the potential to address long-standing research challenges, as discussed in [84]. In [85], a two-step event-driven MFPC strategy is designed by combining a critic NN with an actor NN. This approach aims to overcome limitations arising from system uncertainties and unnecessary switching losses. Currently, these techniques are applied in power converters, but they hold significant potential for use in motor drives as well.

Given the limited processor resources, several offline-trained NNs, such as ANNs mentioned in [34], are also incorporated into the prediction process, and these methods have similarly demonstrated satisfactory control performances. However, the tolerance should be discussed for these NNs, according to their comprehensive performances, since they cannot be actively adjusted to adapt time-varying physics in the motors.

Although NN has the aforementioned advantages, it should recognize that there is ongoing debate about whether NNs belong to data-driven models in MFPC. The primary concern is that the prediction accuracy of NNs has a theoretical upper bound, which does not exceed the accuracy of the training data generation method. This can compromise the stability, convergence, and robustness of the control system, especially if the training data contains parameter mismatches. Besides, NN belongs to interdisciplinary, with independent review articles, such as [86] and [87], including more sufficient research and analysis.

TABLE I
Comparison of MBPC and MFPC

	MBPC	MFPC
Model type	Physical model	Data-driven model
Implementation	Easy	Normal
Robustness	Fair	Strong
Computational burden	Light	Middle / Heavy

VII. Comparisons and Possible Applications

A. Comparisons

A basic comparison between MBPC and MFPC is listed in Table I. With the employment of data-driven models in MFPC, the influences stemming from physical parameters and their negative impacts are entirely mitigated, thus enhancing the robustness of the system. However, this comes at the price of more complex implementation and heavier computational burdens during the estimation and prediction processes. This highlights a tradeoff between processor resources and model orders. On one hand, model orders must be selected based on the available processor resources. On the other hand, the optimal values for achieving the best performance continuously change under different operating states, suggesting that more flexible order selections should be considered.

To estimate computational times and model complexities for typical strategies, some tests are conducted on MBPC and some MFPCs. The results, shown in Fig. 20, are averages from four repeated experiments to reduce randomness, approximately showing the computational time for various models. Based on these results, a comparative analysis of some typical data-driven models in MFPC is presented in Table II, and Table III summarizes some features of them. According to the aforementioned characteristics of these models, they are all formulated based on sample data or its gradient, effectively eliminating the presence of physical parameters and enhancing system robustness. Especially, except for some ULM-based MFPCs, other strategies achieve total model-freeness, essentially enhancing robustness.

TABLE II
COMPARISON TYPICAL MFPCS WITH SOME TYPICAL MODELS

	Single model structures				Flexible model structures	
	Ultra-local	Time-series	LUT	Dynamic-linearization	RNN	ANN
Model type	Data-driven model	Data-driven model	Data-driven model	Data-driven model	Neural network	Neural network
Data type	Sample data	Sample data	Data gradient	Data gradient	Optional	Optional
Implementation	Easy	Normal	Easy	Easy	Hard	Hard
Training data length	Short	Normal	Short	Short	Long	Long
Computational burden	Light	Normal	Light	Light	Heavy	Heavy
Prediction error	Normal	Normal/Good [a]	Normal	Normal	Good	Good
Model flexibility	Fixed	Fixed [b]	Fixed	Fixed	Variable [c] (training process only)	Variable (training process only)
Rough radar images [d]	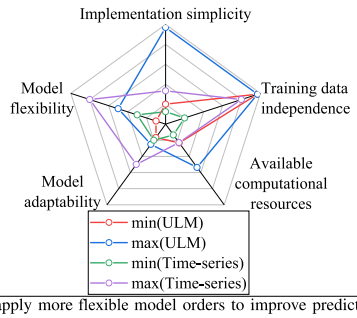		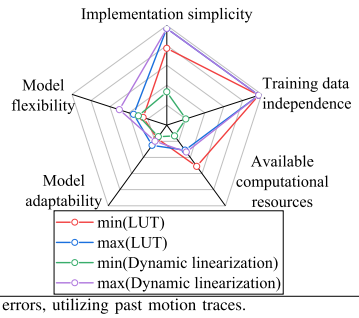		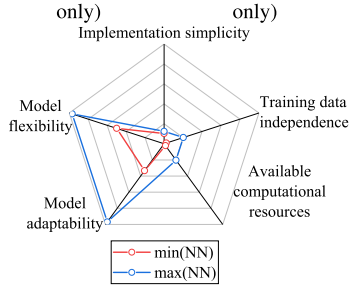	

[a] Considering time-series can apply more flexible model orders to improve prediction errors, utilizing past motion traces.
[b] Although an adaptive law is designed in [33] to adjust model orders online, there is no essential change or improvement in the model structure.
[c] Cannot obtain a specific network structure due to the limited mathematical theory for NNs.
[d] The coverage range of the radar images is only one possibility provided. These images should be used as a rough reference only.

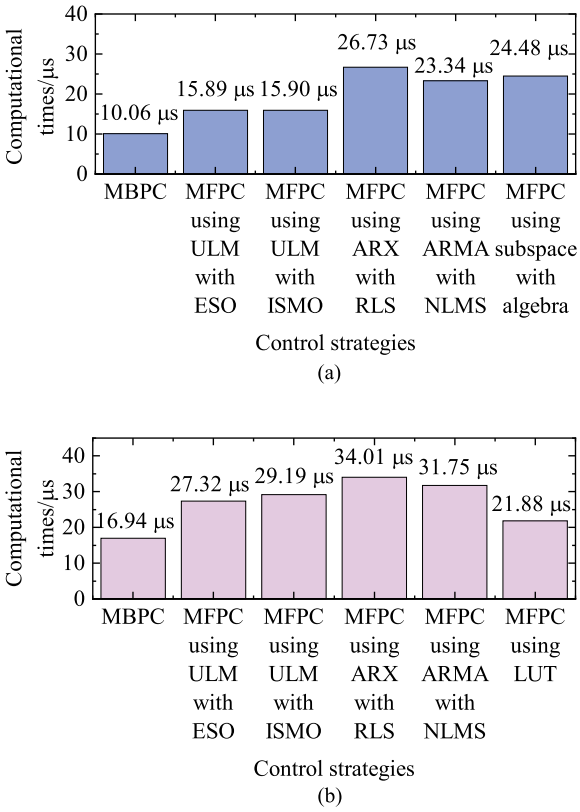

Fig. 20. Computational times for MBPC and some typical MFPCs. (a) CCS-type. (b) FCS-type.

For the time-series model, owing to its consideration of the time properties of motor drives, it can achieve good model adaptability and prediction accuracy at the cost of a degree of computational burdens . Nonetheless, the required resources and the length of training data are not excessively increased compared to those required by neural networks, indicating that MFPC using time-series strikes a balance among these methodologies.

The applications of these models in MFPCs are also summarized in Table III for various types of motors, including PMSM, induction motors (IM), switched reluctance motors (SRM), and linear motors (LM), among others. Since these motors share similar causal relationships, these models should not be limited by motor type in theory and should have a wide range of practical applications. In addition, some models have special applications, such as low-speed operation in [88], high-load overmodulation in [89] and [90], and suppressing common-mode voltages in [91] by improving estimations.

B. *Possible Applications and Open Problems of MFPC*

Beyond PMSM drives, MFPC has also been used to various motor driving systems, including induction motors, reluctance motors, and dc motors. While it has shown enhanced robustness in these applications, there is still room for improvement in different scenarios, where open problems persist.

1) High-End Applications (Data Enhancement): In high-end applications, in addition to robustness, stability and prediction accuracy are also essential indicators in the system, and better model adaptability is the goal that MFPC constantly pursues. In most operating states, predictive control based on physical models can achieve good performance. It can be considered that combining the advantages of physical models to improve the performance of MFPC fully meets the requirements of high-end applications. As shown in Fig. 21, there are many transitional studies between physical models and data-driven models, such as the learning of unknown or unmodeled physical terms (delta learning unknown physics and delta learning physics corrector),

TABLE III
SUMMARY OF SOME TYPICAL MFPCS

Data-driven model	Implementation in Refs. [e]	Applied Motors	Unified converging	Totally model-free	Estimation algorithms	Features
Ultra-local model	FCS/CCS (PCC,PSC,PTC)	PMSM, IM, SRM, LM, BLDC [f]	× [a]	×	Observers	1. Required parameters are γ, $\boldsymbol{F}$ and observer parameters. 2. The gains often need to be selected based on physics. 3. Good converging rate of observers. 4. Simple implementation estimating state variables.
				◯	KF, RLS, Algebraic Data gradient	1. Required parameters are γ, $\boldsymbol{F}$ and estimation parameters, such as the forgetting factor in the RLS algorithm. 2. Eliminate the dependance on physics, and enhance robustness.
Time-series model	FCS/CCS (PCC)	PMSM	◯	◯	RLS, LMS, RGC	1. Required parameters are model coefficients and estimation parameters, such as the forgetting factor in the RLS algorithm. 2. Eliminate the dependance on physics, and enhance robustness. 3. Fair converging rate of commonly used estimation algorithms. 4. Requires more processor resources in the estimation process, and more suit for CCS-type.
LUT	FCS/CCS (PCC)	PMSM, SRM	◯	◯	Data gradient	1. Group tables based on the data gradients and candidate vectors. 2. Eliminate the dependance on physics, and enhance robustness. 3. Good converging rate of direct grouped tables. 4. Simple implementation updating tables. 5. Stagnation effect becomes a primary issue.
Dynamic -linearization model	FCS/CCS (PCC)	PMSM, BLDC, LM	- [b]	◯	PPD bounded estimation	1. Required parameters are model coefficients and estimation parameters. 2. Eliminate the dependance on physics, and enhance robustness. 3. Good converging rate of PPD estimation. 4. Simple implementation estimating state variables.
Multi-models	CCS (PCC)	PMSM, IM	◯ [c1]	◯ [c2]	Optional [d]	1. Required parameters are model coefficients and estimation parameters, such as the forgetting factor in the RLS algorithm. 2. Eliminate the dependance on physics, and enhance robustness, if all sub-models are data-driven. 3. Requires more processor resources in the estimation process, and more suit for CCS-type.
NNs	FCS/CCS (PCC, PPC)	PMSM, SRM	-	◯	Training data	1. Required parameters are factors in NN mainly. 2. Eliminate the dependance on physics, and enhance robustness. 3. Requires more processor resources in the updating process. 4. Requires more training data to generate initial networks, where exists an upper bound of adaptability based on the training data.

[a] According to their relating physical and electrical parameters, the gains γ, ι and lumped variable $\boldsymbol{F}$ require different converging rate, where the label of × reflects an issue that should be considered when applying this model, and ◯ means that meets this criterion. Perhaps using two or more different estimations would be more appropriate for improving model adaptability.
[b] The PPD time-varying vectors ensure bounded system only, but cannot clearly judge converging rates of each terms for now.
[c1],[c2] The unified converging rate and totally model-free are only confirmed for the method in [80]. The specific state is determined by the selected sub-model structure.
[d] The estimation algorithm should be selected according to the structure of sub-models for the multi-models.
[e] PCC, PSC, PTC and PPC reflect predictive current control, predictive speed control, predictive torque control and predictive position control respectively, based on the mentioned references.
[f] IM, SRM, LM and BLDC reflect induction motor, switched reluctance motor, linear motor and brushless DC motor respectively, involving 3-phase, open-end winding, dual 3-phase and multi-phase types, based on the mentioned references.

and introduction of physical principles at the model level or during the modeling process (physics encoded, physics guided, and physics constrained).

Although MFPC completely eliminates the dependence on physical parameters, the adaptability of data-driven models heavily depends on the quality of data. According to the basic structure shown in Fig. 2, the data-driven model should only describe the plant and measurement devices within the motor driving system. However, some components in the sample data have had adverse effects on the accuracy of the model, including some high-frequency harmonics resulting from coupling and side-frequency effects, and disturbances caused by position errors. These components originate from the control strategy and modulation process. Implementing

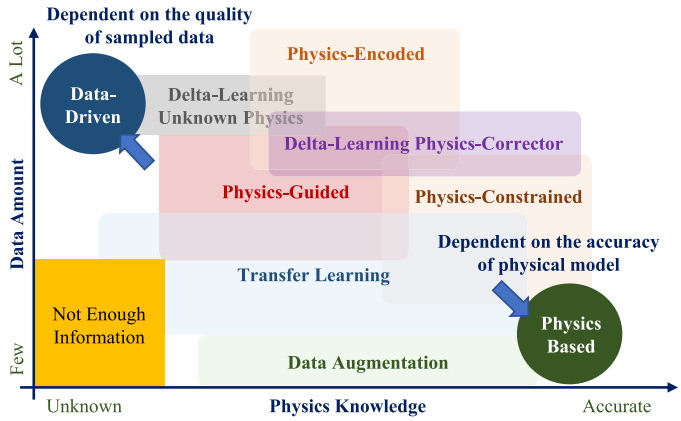

Fig. 21. Sketch diagram of transitional research between physical models and data-driven models.

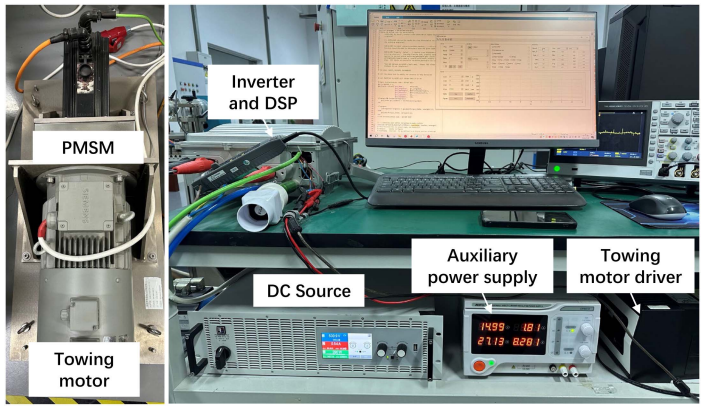

Fig. 22. Structure of experimental platform.

an extraction filter to mitigate the adverse effects of these unnecessary components is crucial for achieving data cleaning or enhancement.

Based on the aforementioned analysis, here is an open problem for MFPC. High-power motors generally have lower inductance and resistance compared to low-power motors. This difference could impact the behavior of the control system, particularly in terms of the signal-noise ratio during current measurements. The robustness of MFPC strategies under these conditions might remain unaddressed, and the data enhancement may be an effective solution.

2) Imbalanced Grid Faults: After long-distance power transmission, the grid often weakens, causing imbalance faults in grid-connected motor drives. Since most motors are based on three-phase or six-phase configurations, such as permanent-magnet motors and induction motors, which typically exhibit symmetric coordinate systems, the typical control strategies cannot maintain a balanced operating state and prevent further exacerbation of faults. Under conditions of driver imbalance, MFPC may perform well in achieving better performance and lower degree of imbalance because of the continuous updating of its data model, and minimize the possibility of local heating and motor failures caused by these faults. Due to the characteristic and the superior dynamics of predictive control, MFPC-based systems can quickly recover to normal operating state if the fault is resolved, and have great potential for application in scenarios with high grid-connected motor drive failure rates. In addition, some grid-connected motor drives require greater inertia, to prevent disconnection in the event of a fault and maintain reliable system operation. Some adaptive inertia-based MFPCs may provide a solution to achieve this requirement.

3) Efficiency Improvement: In industry, about 60% of electrical energy is consumed by motor drives, and it is crucial to enhance efficiency and reduce energy consumption. The physical models and data-driven models are mainly designed based on the motion characteristics of the plant. If some loss models could be involved in the data-driven model structure or estimation algorithm in MFPC, and the cost function terms are also improved to optimize the losses, the operating efficiency may be enhanced effectively in the system.

VIII. Conclusion

This article explores various data-driven models in MFPCs for motor drives, emphasizing their ability to mitigate model parameter mismatch and enhance robustness and stability across different operating points. Through a novel classification based on implementation and discussion methods, research evaluates the advantages and challenges of different MFPC models, including signal model structure based on direct data and data gradient, transitional model structure, and flexible model structure. Although the MFPC strategies still has various limitations, they overall show great promise for excellent control performances and broader application spaces. Unique contributions of this article include: a fresh perspective on MFPC from the predictive control theory, a novel classification of MFPCs based on data-driven model structures, unique insights on performance analyses, and a comprehensive summary of MFPC research, which fills gaps in the existing literature.

Appendix A
Appendix Experimental Setup Descriptions and Design Samples for MFPCs

The experimental platform, shown in Fig. 22, is based on a 4.8-kW PMSM. The control core of this setup is a DSP (F28379D), and it is powered by a three-phase inverter equipped with insulated-gate bipolar transistors (FF600R12ME4). To generate load torques, a towing motor driven by an ABB driver is utilized. For a comprehensive overview of the experimental setup, refer to Table IV, which lists key information of the motor and its system.

It should be noted that during the experiment processes, the measurement is designed to capture instantaneous current values, which are then sampled by current sensors and transferred to the host computer via the SCI port of DSP. The sampled data are then used for analysis, without specific consideration for peak or mean values. While an oscilloscope and external current probe

TABLE IV
KEY INFORMATION ABOUT EXPERIMENTAL SETUP

Symbols	Quantity	Values
R_s	Stator resistance	0.637 Ω
L_{sd}	Stator inductance on d-axis	10 mH
L_{sq}	Stator inductance on q-axis	14.5 mH
p	Number of pole pairs	4
ψ_m	Magnetic flux linkage	0.31 Wb
J	Rotor inertia	0.005 kg·m^2
$V_{\rm dc}$	DC voltage	540 V
T_s	Sampling period	62.5 μs

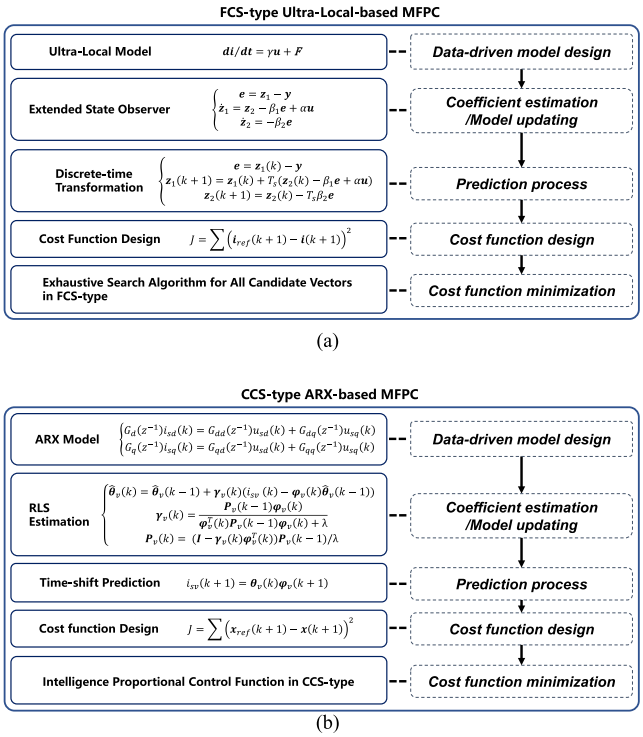

Fig. 23. Implementation for some MFPCs. (a) FCS-type ultralocal-based MFPC. (b) CCS-type ARX-based MFPC.

are used for observation during experiments, they are not the primary tools for data acquisition.

Because of limited processor resources, some of the results are tested using MATLAB simulation software. All design parameters are carefully set to match the experimental platform parameters.

To facilitate understanding of the implementation process of MFPC, here are two design samples. Specifically, Fig. 23 presents the FCS-type ultralocal-based MFPC and the CCS-type ARX-based MFPC. This article focuses on the model designing, updating and prediction within the first three steps of the implementation process.

REFERENCES

[1] M. Gu et al., "Finite control set model predictive torque control with reduced computation burden for PMSM based on discrete space vector modulation," *IEEE Trans. Energy Convers.*, vol. 38, no. 1, pp. 703–712, Mar. 2023.

[2] J. Rodriguez et al., "Latest advances of model predictive control in electrical drives—Part I: Basic concepts and advanced strategies," *IEEE Trans. Power Electron.*, vol. 37, no. 4, pp. 3927–3942, Apr. 2022.

[3] M. F. Elmorshedy, W. Xu, F. F. M. El-Sousy, M. R. Islam, and A. A. Ahmed, "Recent achievements in model predictive control techniques for industrial motor: A comprehensive state-of-the-art," *IEEE Access*, vol. 9, pp. 58170–58191, 2021.

[4] Z. Hou and Z. Wang, "From model-based control to data-driven control: Survey, classification and perspective," *Inf. Sci.*, vol. 235, pp. 3–35, Jun. 2013, doi: 10.1016/j.ins.2012.07.014.

[5] G. Bramerdorfer, G. Lei, A. Cavagnino, Y. Zhang, J. Sykulski, and D. A. Lowther, "More robust and reliable optimized energy conversion facilitated through electric machines, power electronics and drives, and their control: State-of-the-art and trends," *IEEE Trans. Energy Convers.*, vol. 35, no. 4, pp. 1997–2012, Dec. 2020.

[6] Y. Shi and K. Zhang, "Advanced model predictive control framework for autonomous intelligent mechatronic systems: A tutorial overview and perspectives," *Annu. Rev. Control*, vol. 52, pp. 170–196, 2021, doi: 10.1016/j.arcontrol.2021.10.008.

[7] L. Xu et al., "Robust predictive current control of hybrid-excited axial flux-switching PM motor based on multiple-resolution parameter identification," *IEEE Trans. Ind. Electron.*, vol. 71, no. 11, pp. 13708–13719, Nov. 2024, doi: 10.1109/TIE.2024.3374390.

[8] A. Brosch, O. Wallscheid, and J. Böcker., "Long-term memory recursive least squares online identification of highly utilized permanent magnet synchronous motors for finite-control-set model predictive control," *IEEE Trans. Power Electron.*, vol. 38, no. 2, pp. 1451–1467, Feb. 2023.

[9] X. Sun, X. Lin, D. Guo, G. Lei, and M. Yao, "Improved deadbeat predictive current control with extended state observer for dual three-phase PMSMs," *IEEE Trans. Power Electron.*, vol. 39, no. 6, pp. 6769–6782, Jun. 2024.

[10] X. Li, W. Tian, Q. Yang, P. Karamanakos, and R. Kennel, "Augmented multistep finite-control-set model predictive control for induction motor-drive system," *IEEE Trans. Power Electron.*, vol. 38, no. 11, pp. 13842–13854, Nov. 2023.

[11] J. Lei, S. Fang, D. Huang, D. Huang, and Y. Wang, "Enhanced deadbeat predictive current control for PMSM drives using iterative sliding mode observer," *IEEE Trans. Power Electron.*, vol. 38, no. 11, pp. 13866–13876, Nov. 2023.

[12] M. S. Mousavi et al., "Predictive torque control of induction motor based on a robust integral sliding mode observer," *IEEE Trans. Ind. Electron.*, vol. 70, no. 3, pp. 2339–2350, Mar. 2023.

[13] M. Khalilzadeh, S. Vaez-Zadeh, J. Rodriguez, and R. Heydari, "Model-free predictive control of motor drives and power converters: A review," *IEEE Access*, vol. 9, pp. 105733–105747, 2021.

[14] I. Markovsky, L. Huang, and F. Dörfler, "Data-driven control based on the behavioral approach: From theory to applications in power systems," *IEEE Control Syst.*, vol. 43, no. 5, pp. 28–68, Oct. 2023.

[15] C. Ma et al., "A direct optimal input determination data-based predictive current control for PMSM drives without system identification," *IEEE J. Emerg. Sel. Topics Power Electron.*, vol. 12, no. 3, pp. 2707–2717, Jun. 2024.

[16] Y. Zhang, J. Jin, and L. Huang, "Model-free predictive current control of PMSM drives based on extended state observer using ultralocal model," *IEEE Trans. Ind. Electron.*, vol. 68, no. 2, pp. 993–1003, Feb. 2021.

[17] B. Xu, Q. Wu, J. Ma, X. Liu, and Y. Fang, "Improved non-cascaded continuous-set model-free predictive control scheme for PMSM drives," *IET Power Electron.*, vol. 18, 2025, Art. no. e12830, doi: 10.1049/pel2.12830.

[18] J. Kang, X. Huang, C. Xia, D. Huang, and F. Wang, "Ultralocal model-free adaptive supertwisting nonsingular terminal sliding mode control for magnetic levitation system," *IEEE Trans. Ind. Electron.*, vol. 71, no. 5, pp. 5187–5194, May 2024.

[19] J. Liu, Y. Yang, X. Li, K. Zhao, Z. Yi, and Z. Xin, "Improved model-free continuous super-twisting non-singular fast terminal sliding mode control of IPMSM," *IEEE Access*, vol. 11, pp. 85361–85373, 2023.

[20] Y. Wei, H. Young, D. Ke, F. Wang, and J. Rodríguez, "Model-free predictive current control using extended affine ultralocal for PMSM drives," *IEEE Trans. Ind. Electron.*, vol. 71, no. 7, pp. 6719–6729, Jul. 2024.

[21] Z. Sun, Y. Deng, J. Wang, T. Yang, Z. Wei, and H. Cao, "Finite control set model-free predictive current control of PMSM with two voltage vectors based on ultralocal model," *IEEE Trans. Power Electron.*, vol. 38, no. 1, pp. 776–788, Jan. 2023.

[22] Z. Sun, Y. Deng, J. Wang, H. Li, and H. Cao, "Improved cascaded model-free predictive speed control for PMSM speed ripple minimization based on ultra-local model," *ISA Trans.*, vol. 143, pp. 666–677, Dec. 2023, doi: 10.1016/j.isatra.2023.10.008.

[23] Y. Wei, H. Young, F. Wang, and J. Rodríguez, "Generalized data-driven model-free predictive control for electrical drive systems," *IEEE Trans. Ind. Electron.*, vol. 70, no. 8, pp. 7642–7652, Aug. 2023.

[24] R. Heydari et al., "Model-free predictive control of grid-forming inverters with LCL filters," *IEEE Trans. Power Electron.*, vol. 37, no. 8, pp. 9200–9211, Aug. 2022.

[25] H. Yang, Y. Zhang, and W. Shen, "Predictive current control and field-weakening operation of SPMSM drives without motor parameters and DC voltage," *IEEE J. Emerg. Sel. Topics Power Electron.*, vol. 10, no. 5, pp. 5635–5646, Oct. 2022.

[26] P. G. Carlet, F. Tinazzi, S. Bolognani, and M. Zigliotto, "An effective model-free predictive current control for synchronous reluctance motor drives," *IEEE Trans. Ind. Appl.*, vol. 55, no. 4, pp. 3781–3790, Jul./Aug. 2019.

[27] T. Rui et al., "Modulated model-free predictive current control for voltage source inverters with stagnation elimination and sampling disturbance suppression," *IEEE Trans. Power Electron.*, vol. 38, no. 6, pp. 6996–7008, Jun. 2023.

[28] L. Duan, Z. Hou, X. Yu, S. Jin, and K. Lu, "Data-driven model-free adaptive attitude control approach for launch vehicle with virtual reference feedback parameters tuning method," *IEEE Access*, vol. 7, pp. 54106–54116, 2019.

[29] X. Zhang, Z. Liu, P. Zhang, and Y. Zhang, "Model predictive current control for PMSM drives based on nonparametric prediction model," *IEEE Trans. Transport. Electrific.*, vol. 10, no. 1, pp. 711–719, Mar. 2024.

[30] Y. Wei, H. Young, D. Ke, F. Wang, H. Qi, and J. Rodríguez, "Model-free predictive control using sinusoidal generalized universal model for PMSM drives," *IEEE Trans. Ind. Electron.*, vol. 71, no. 11, pp. 13720–13731, Nov. 2024.

[31] A. Brosch, S. Hanke, O. Wallscheid, and J. Böcker, "Data-driven recursive least squares estimation for model predictive current control of permanent magnet synchronous motors," *IEEE Trans. Power Electron.*, vol. 36, no. 2, pp. 2179–2190, Feb. 2021.

[32] Z. Yin, X. Wang, X. Su, Y. Shen, D. Xiao, and H. Zhao, "A switched ultra-local model-free predictive controller for PMSMs," *IEEE Trans. Power Electron.*, vol. 39, no. 9, pp. 10665–10669, Sep. 2024.

[33] Y. Wei, H. Young, D. Ke, D. Huang, F. Wang, and J. Rodríguez, "Adaptive ultralocalized time-series for improved model-free predictive current control on PMSM drives," *IEEE Trans. Power Electron.*, vol. 39, no. 5, pp. 5155–5165, May 2024.

[34] D. Wang et al., "Model predictive control using artificial neural network for power converters," *IEEE Trans. Ind. Electron.*, vol. 69, no. 4, pp. 3689–3699, Apr. 2022.

[35] X. Lin et al., "Observer-based prescribed performance speed control for PMSMs: A data-driven RBF neural network approach," *IEEE Trans. Ind. Inform.*, vol. 20, no. 5, pp. 7502–7512, May 2024.

[36] J. Carrillo-Ríos, I. González-Prieto, Á. González-Prieto, M. J. Durán, and J. J. Aciego, "Long-prediction horizon FCS-MPC for multiphase electric drives with a selective control action promotion," *IEEE Trans. Ind. Electron.*, vol. 71, no. 9, pp. 9982–9993, Sep. 2024.

[37] J. Chen et al., "Computation-efficient model predictive control using sphere decoding algorithm for DTP-PMSMs," *IEEE Trans. Magn.*, vol. 60, no. 10, pp. 1–5, Oct. 2024.

[38] Z. Zhang, J. Chen, R. Han, Y. Wu, Y. Gong, and S. Chang, "K-best-Sphere-Decoding-Based model predictive control for dual three-phase SPMSMs," *IEEE Trans. Magn.*, vol. 60, no. 9, pp. 1–6, Sep. 2024.

[39] A. A. Ahmed, B. K. Koh, and Y. I. Lee, "A comparison of finite control set and continuous control set model predictive control schemes for speed control of induction motors," *IEEE Trans. Ind. Inform.*, vol. 14, no. 4, pp. 1334–1346, Apr. 2018.

[40] X. Wu et al., "Parameter-free predictive torque and flux control for PMSM based on incremental stator flux predictive model," *IEEE Trans. Ind. Inform.*, vol. 20, no. 2, pp. 2715–2726, Feb. 2024.

[41] X. Zhang and L. Xu, "A simple motor-parameter-free model predictive voltage control for PMSM drives based on incremental model," *IEEE J. Emerg. Sel. Topics Power Electron.*, vol. 12, no. 3, pp. 2845–2854, Jun. 2024.

[42] W. A. Manzoor, S. Rawashdeh, and A. Mohammadi, "Vehicular applications of Koopman operator theory—A survey," *IEEE Access*, vol. 11, pp. 25917–25931, Mar. 2023.

[43] W. Li, H. Yuan, S. Li, and J. Zhu, "A revisit to model-free control," *IEEE Trans. Power Electron.*, vol. 37, no. 12, pp. 14408–14421, Dec. 2022.

[44] M. S. Mousavi, S. A. Davari, V. Nekoukar, C. Garcia, and J. Rodriguez, "Integral sliding mode observer-based ultralocal model for finite-set model predictive current control of induction motor," *IEEE J. Emerg. Sel. Topics Power Electron.*, vol. 10, no. 3, pp. 2912–2922, Jun. 2022.

[45] W. Huang, Y. Huang, and D. Xu, "Model-free predictive current control of five-phase PMSM drives," *Electronics*, vol. 12, no. 23, 2023, Art. no. 4848, doi: 10.3390/electronics12234848.

[46] Z. Su, X. Sun, G. Lei, and M. Yao, "Model-free predictive current control for dual three-phase PMSM drives with an optimal modulation pattern," *IEEE Trans. Ind. Electron.*, vol. 71, no. 9, pp. 10140–10149, Sep. 2024.

[47] X. Yuan, Y. Zuo, Y. Fan, and C. H. T. Lee, "Model-free predictive current control of SPMSM drives using extended state observer," *IEEE Trans. Ind. Electron.*, vol. 69, no. 7, pp. 6540–6550, Jul. 2022.

[48] J. Mao et al., "Non-cascaded model-free predictive speed control of SMPMSM drive system," *IEEE Trans. Energy Convers.*, vol. 37, no. 1, pp. 153–162, Mar. 2022.

[49] X. Liu, L. Qiu, Y. Fang, K. Wang, Y. Li, and J. Rodríguez, "A simple model-free solution for finite control-set predictive control in power converters," *IEEE Trans. Power Electron.*, vol. 39, no. 10, pp. 12627–12635, Oct. 2024.

[50] Y. Zhang, W. Shen, and H. Yang, "An improved deadbeat predictive current control of PMSM drives based on the ultra-local model," *Chin. J. Electr. Eng.*, vol. 9, no. 2, pp. 27–37, Jun. 2023, doi: 10.23919/CJEE.2023.000020.

[51] S. Bolognani, P. G. Carlet, F. Tinazzi, and M. Zigliotto, "Current ripple minimisation in deadbeat parameter-free predictive control of synchronous motor drives," *IEEE Open J. Ind. Appl.*, vol. 2, pp. 278–288, 2021.

[52] Z. Liu, X. Huang, Q. Hu, G. Yang, Y. Wang, and J. Shen, "Model-free predictive current control of PMSM using modified extended state observer," *IEEE Trans. Power Electron.*, vol. 40, no. 1, pp. 679–690, Jan. 2025.

[53] N. Yang, S. Zhang, X. Li, and X. Li, "A new model-free deadbeat predictive current control for PMSM using parameter-free luenberger disturbance observer," *IEEE J. Emerg. Sel. Topics Power Electron.*, vol. 11, no. 1, pp. 407–417, Feb. 2023.

[54] R. Moradpour and A. Tavakoli, "Smooth commutation of brushless DC motor by model-free predictive current control without Back-EMF estimation," *IET Electric Power Appl.*, vol. 17, no. 5, pp. 721–729, May 2023, doi: 10.1049/elp2.12299.

[55] C. Zhang et al., "Model-free predictive voltage control of the floating capacitor in hybrid-inverter open- winding permanent magnet synchronous motor," *IEEE Trans. Ind. Electron.*, vol. 71, no. 10, pp. 11925–11935, Oct. 2024.

[56] X. Sun, X. Lin, L. Zhang, M. Yao, and Y. Cai, "An improved torque enhancement strategy for dual three-phase PMSM based on model-free predictive current control," *IEEE Trans. Transport. Electrific.*, vol. 11, no. 1, pp. 176–187, Feb. 2025.

[57] M. S. Mousavi, S. A. Davari, F. Flores-Bahamonde, C. Garcia, and J. Rodriguez, "Sampling error-based model-free predictive current control of open-end winding induction motor with simplified vector selection," *IET Electr. Power Appl.*, vol. 17, pp. 358–369, 2023, doi: 10.1049/elp2.12273.

[58] S. Agoro and I. Husain, "Model-free predictive current and disturbance rejection control of dual three-phase PMSM drives using optimal virtual vector modulation," *IEEE J. Emerg. Sel. Topics Power Electron.*, vol. 11, no. 2, pp. 1432–1443, Apr. 2023.

[59] J. Zhao, Y. Zhang, and X. Wang, "Model-free predictive current control of PMSM drives based on variable sequence space vector modulation using an ultra-local model," *IEEE Trans. Transport. Electrific.*, vol. 10, no. 2, pp. 3518–3528, Jun. 2024.

[60] M. Kermadi et al., "Model-free predictive current controller for voltage source inverters using ARX model and recursive least squares," *IEEE Trans. Circuits Syst. II, Exp. Briefs*, vol. 71, no. 5, pp. 2619–2623, May 2024.

[61] Y. Wei et al., "Low prediction error model-free predictive control on PMSM drives with ordinary kriging time-shift," *IEEE Trans. Transport. Electrific.*, early access, Jan. 7, 2025, doi: 10.1109/TTE.2025.3526791.

[62] P. G. Carlet, A. Favato, S. Bolognani, and F. Dörfler, "Data-driven continuous-set predictive current control for synchronous motor drives," *IEEE Trans. Power Electron.*, vol. 37, no. 6, pp. 6637–6646, Jun. 2022.

[63] M. Lazar and P. C. N. Verheijen, "Generalized data–driven predictive control: Merging subspace and Hankel predictors," *Mathematics*, vol. 11, no. 9, 2023, Art. no. 2216, doi: 10.3390/math11092216.

[64] Y. Feng, S. Zhang, and C. Zhang, "An improved model-free predictive current control for PMSM under low-speed condition," *IEEE J. Emerg. Sel. Topics Power Electron.*, vol. 12, no. 1, pp. 555–565, Feb. 2024.

[65] L. Luo, F. Yu, L. Ren, and C. Lu, "Parameter-free model predictive current control for PMSM based on current variation estimation without position sensor," *Energies*, vol. 16, no. 19, 2023, Art. no. 6792, doi: 10.3390/en16196792.
[66] C. Ma, J. Rodriguez, C. Garcia, and F. De Belie, "Integration of reference current slope based model-free predictive control in modulated PMSM drives," *IEEE J. Emerg. Sel. Topics Power Electron.*, vol. 11, no. 2, pp. 1407–1421, Apr. 2023.
[67] M. Pereira and R. E. Araujo, "Model-free finite-set predictive current control with optimal cycle time for a switched reluctance motor," *IEEE Trans. Ind. Electron.*, vol. 70, no. 8, pp. 8355–8364, Aug. 2023.
[68] P. G. Ipoum-Ngome et al., "Multiobjective model-free predictive control for motor drives and grid-connected applications: Operating with unbalanced multilevel cascaded H-bridge inverters," *IEEE Trans. Power Electron.*, vol. 38, no. 3, pp. 3014–3028, Mar. 2023.
[69] F. Wang, Y. Wei, H. Young, D. Ke, X. Yu, and J. Rodríguez, "Low-stagnation model-free predictive current control of PMSM drives," *IEEE Trans. Ind. Electron.*, early access, Dec. 11, 2024, doi: 10.1109/TIE.2024.3508070.
[70] F. Yu, C. Zhou, X. Liu, and C. Zhu, "Model-free predictive current control for three-level inverter-fed IPMSM with an improved current difference updating technique," *IEEE Trans. Energy Convers.*, vol. 36, no. 4, pp. 3334–3343, Dec. 2021.
[71] C. Ma, H. Li, X. Yao, Z. Zhang, and F. De Belie, "An improved model-free predictive current control with advanced current gradient updating mechanism," *IEEE Trans. Ind. Electron.*, vol. 68, no. 12, pp. 11968–11979, Dec. 2021.
[72] C. A. Agustin, J. -T. Yu, Y.-S. Cheng, C. K. Lin, and Y. W. Yi, "A synchronized current difference updating technique for model-free predictive current control of PMSM drives," *IEEE Access*, vol. 9, pp. 63306–63318, 2021.
[73] D. Velmurugan, A. Arumugam, C. -K. Lin, C. A. Agustin, and J. C. Chen, "Improved triple-voltage-vector model-free predictive current control for synchronous reluctance motor drives," *IEEE Access*, vol. 12, pp. 68109–68129, 2024.
[74] B. Luo, X. Yang, and Y. Zhou, "Model-free predictive current control of permanent magnet synchronous motor based on estimation of current variations," *IEEE Trans. Ind. Electron.*, vol. 71, no. 8, pp. 8395–8405, Aug. 2024.
[75] M. Khalilzadeh, S. Vaez-Zadeh, and M. S. Eslahi, "Parameter-free predictive control of IPM motor drives with direct selection of optimum inverter voltage vectors," *IEEE J. Emerg. Sel. Topics Power Electron.*, vol. 9, no. 1, pp. 327–334, Feb. 2021.
[76] X. Wang, Y. Zhang, and C. Li, "Research on model-free adaptive control of electro-hydraulic servo system of continuous rotary motor," *IEEE Access*, vol. 10, pp. 31165–31174, 2022.
[77] X. Wang, S. Yao, and C. Qu, "PPMLM direct thrust force control based on iterative learning high-order improved model free adaptive control," *IET Renewable Power Gener.*, vol. 18, no. 9–10, pp. 1661–1674, Jul. 2024, doi: 10.1049/rpg2.13013.
[78] W. Wu, L. Qiu, X. Liu, J. Ma, J. Rodriguez, and Y. Fang, "Dynamic-linearization-Based predictive control of a voltage-source inverter," *IEEE Trans. Ind. Electron.*, vol. 71, no. 4, pp. 3275–3284, Apr. 2024.
[79] H. Yang, K. Zhang, and X. Wang, "Multi-model switching predictive control with active fault tolerance for high-speed train," *Control Theory Appl.*, vol. 29, no. 9, pp. 1211–1214, 2012.
[80] S. Zhang, O. Wallscheid, and M. Porrmann, "Machine learning for the control and monitoring of electric machine drives: Advances and trends," *IEEE Open J. Ind. Appl.*, vol. 4, pp. 188–214, 2023.
[81] H. Mesai Ahmed, I. Jlassi, A. J. Marques Cardoso, and A. Bentaallah, "Model-free predictive current control of synchronous reluctance motors based on a recurrent neural network," *IEEE Trans. Ind. Electron.*, vol. 69, no. 11, pp. 10984–10992, Nov. 2022.
[82] N. Tan, P. Yu, Z. Zhong, and F. Ni, "A new noise-tolerant dual-neural-network scheme for robust kinematic control of robotic arms with unknown models," *IEEE/CAA J. Automatica Sinica*, vol. 9, no. 10, pp. 1778–1791,Oct. 2022.
[83] S. Sabzevari, R. Heydari, M. Mohiti, M. Savaghebi, and J. Rodriguez, "Model-free neural network-based predictive control for robust operation of power converters," *Energies*, vol. 14, no. 8, 2021, Art. no. 2325, doi: 10.3390/en14082325.
[84] X. Liu, L. Qiu, Y. Fang, K. Wang, Y. Li, and J. Rodríguez, "Combining data-driven and event-driven for online learning predictive control in power converters," *IEEE Trans. Power Electron.*, vol. 40, no. 1, pp. 563–573, Jan. 2025.
[85] X. Liu, L. Qiu, Y. Fang, K. Wang, Y. Li, and J. Rodríguez, "Event-driven based reinforcement learning predictive controller design for three-phase NPC converters using online approximators," *IEEE Trans. Power Electron.*, vol. 40, no. 4, pp. 4914–4926, Apr. 2025.
[86] W. Qiu, X. Zhao, A. Tyrrell, S. Perinpanayagam, S. Niu, and G. Wen, "Application of artificial intelligence-based technique in electric motors: A review," *IEEE Trans. Power Electron.*, vol. 39, no. 10, pp. 13543–13568, Oct. 2024.
[87] M. Monadi, M. Nabipour, F. Akbari-Behbahani, and E. Pouresmaeil, "Speed control techniques for permanent magnet synchronous motors in electric vehicle applications toward sustainable energy mobility: A review," *IEEE Access*, vol. 12, pp. 119615–119632, 2024.
[88] Y. Feng et al., "An improved model-free predictive current control for PMSM drives based on current circle tracking under low-speed conditions," *IEEE Access*, vol. 12, pp. 57767–57779, Apr. 2024.
[89] X. Wu, B. Chen, M. Yang, T. Wu, S. Huang, and H. Cui, "Improved model-free predictive current control method for SPMSM with an overmodulation scheme," *IEEE Trans. Ind. Electron.*, vol. 71, no. 8, pp. 8427–8437, Aug. 2024.
[90] Z. Zhu, X. Wei, F. Yu, and Z. Zhang, "Overmodulatable parameter-free predictive current control for PMSMs," *IEEE Trans. Power Electron.*, vol. 40, no. 1, pp. 1774–1786, Jan. 2025.
[91] S. Agoro and I. Husain, "Model predictive control with double virtual vector modulation for suppressing common mode voltages in dual three-phase drives," *IEEE Trans. Ind. Electron.*, vol. 71, no. 9, pp. 10018–10028, Sep. 2024.

Fengxiang Wang (Senior Member, IEEE) was born in Jiujiang, China, in 1982. He received the B.S. degree in electronic engineering and the M.S. degree in automation from Nanchang Hangkong University, Nanchang, China, in 2005 and 2008, respectively, and the Ph.D. degree in electrical engineering from the Institute for Electrical Drive Systems and Power Electronics, Technische Universitaet Muenchen, Munich, Germany, in 2014.

He is currently a Full Professor and the Director with Quanzhou Institute of Equipment Manufacturing, Haixi Institutes, Chinese Academy of Sciences, Quanzhou, China. His research interests include predictive control and sensorless control for electrical drives and power electronics.

Dr. Wang is an IET Fellow, and an Associate Editor for IEEE TRANSACTIONS ON INDUSTRIAL ELECTRONICS and IEEE TRANSACTIONS ON ENERGY CONVERSION. As the General Chair, he organized the IEEE 5th International Symposium on Predictive Control of Electrical Drives and Power Electronics (PRECEDE).

Yao Wei (Member, IEEE) was born in Handan, China, in 1993. He received the B.S. and Ph.D. degrees in power electronics and power transmission from Yanshan University, Qinhuangdao, China, in 2015 and 2021, respectively.

From 2021 to 2024, he was involved in a postdoctoral project with Quanzhou Institute of Equipment Manufacturing, Haixi Institutes, Chinese Academy of Sciences, Jinjiang, China, where he is currently working as an Assistant Researcher. His research interests include driving and advanced control for electric vehicles and servo systems.

Dr. Wei is a Senior Member of China Electrotechnical Society (CES), a Member of the Chinese Society for Electrical Engineering (CSEE), and a Member of Chinese Association of Automation (CAA).

Jose Rodriguez (Life Fellow, IEEE) received the Engineer degree in electrical engineering from the Universidad Tecnica Federico Santa Maria, Valparaiso, Chile, in 1977, and the Dr.-Ing. degree in electrical engineering from the University of Erlangen, Erlangen, Germany, in 1985.

He has been with the Department of Electronics Engineering, Universidad Tecnica Federico Santa Maria, since 1977, where he was a full Professor and President. From 2015 to 2019, he was the President of Universidad Andres Bello in Santiago, Chile. From 2022 to 2023, he was the President with Universidad San Sebastian, Santiago, Chile, where he is currently the Director of the Center for Energy Transition. He has coauthored two books, several book chapters and more than 1000 journal and conference papers. His main research interests include multilevel inverters, new converter topologies, control of power converters, and adjustable-speed drives.

Dr. Rodriguez was the recipient of a number of Best Paper awards from journals of the IEEE, the National Award of Applied Sciences and Technology from the Government of Chile in 2014, and the Eugene Mittelmann Award from the Industrial Electronics Society of the IEEE in 2015. He is a Member of the Chilean Academy of Engineering. From 2014 to 2024, he was included in the list of Highly Cited Researchers published by Web of Science.

Cristian Garcia (Senior Member, IEEE) received the M.Sc. and Ph.D. degrees in electronics engineering from the Universidad Tecnica Federico Santa Maria, Valparaiso, Chile, in 2013 and 2017, respectively.

In 2016, he was a visiting Ph.D. student with the Power Electronics Machines and Control (PEMC) Group, University of Nottingham, U.K. From 2017 to 2019, he was with the Engineering Faculty, Universidad Andres Bello, Santiago, Chile, as an Assistant Professor. Since 2019, he has been with the Department of Electrical Engineering, University of Talca, Curico, Chile, where he is currently an Assistant Professor. His research interests include electric transportation applications, variable-speed drives, and model predictive control of power converters and drives.

Dr. Garcia is an Associate Editor for IEEE TRANSACTIONS ON TRANSPORTATION ELECTRIFICATION.